Calibration and Parametric Study of the Alcator C-Mod Charge Exchange Neutral Particle Analyzers

by

Jody Christopher Miller

B.S., Nuclear Engineering, Purdue University(1992)

Submitted to the Department of Nuclear Engineering
in partial fulfillment of the requirements for the degree of

Master of Science

at the

MASSACHUSETTS INSTITUTE OF TECHNOLOGY

February 1995

Signature of Author 1/31/95
Department of Nuclear Engineering
January 31, 1995

Certified by 1/31/95
Réjean Boivin
Research Scientist, Plasma Fusion Center
Thesis Supervisor

Certified by 1/31/95
Kevin Wenzel
Assistant Professor, Department of Nuclear Engineering
Thesis Reader

Accepted by .....
Allan F. Henry
Chairman, Departmental Graduate Committee

Calibration and Parametric Study of the Alcator C-Mod Charge Exchange Neutral Particle Analyzers

by

Jody C. Miller

Submitted to the Department of Nuclear Engineering
on January 31, 1995, in partial fulfillment of the
requirements for the degree of
Master of Science

ABSTRACT

The calibration and a parametric study of the Alcator C-Mod charge exchange neutral particle analyzers have been performed. The calibration was done in two parts, the first part examined the field configurations and the second determined the relative efficiencies of the detectors. The charge exchange analyzer unfolds the charge exchange neutral particle flux to give the ion velocity distribution. A bounce averaged, quasilinear, Fokker-Planck computer code was used to generate the charge exchange neutral particle fluxes upon which the parametric study is based. The temperature which the charge exchange analyzers would be expected to measure from the neutral particle fluxes was then compared to the plasma temperature which used to generate the fluxes. It has been determined that charge exchange analysis will underpredict temperatures for the plasma conditions which were studied.

Thesis Supervisor: Réjean Boivin
Title: Research Scientist, Plasma Fusion Center

Thesis Reader: Kevin Wenzel
Title: Assistant Professor, Department of Nuclear Engineering

Contents

Chapter 1

Introduction

Confined fusion is a method of energy generation currently being researched as an energy supply of the future. It represents a clean method of power production with no long term supply problems. With the diminishing supplies of fossil fuels, the increase in world power demand, and the environmental concerns of both fossil fuels and nuclear fission reactors, the importance of a clean energy supply is clear. The renewable sources of hydro-electric, solar, and wind power have limitations depending upon the climate, and are not conducive to space propulsion uses. Fusion energy could solve both of these problems.

The magnetically confined fusion scheme confines energetic charged particles with a strong magnetic field. The current generation of magnetic fusion devices are mainly Tokamaks, whose main magnetic field connects back into itself, making a torus. A complex array of secondary magnets provide equilibrium, stability, and plasma shaping magnetic fields.

To heat the initial gas to a plasma, an inner transformer coil conducts current to produce a loop voltage. The loop voltage produced, 1-2 volts, is on the order of the electron binding energy, 13.6 eV. This accelerates the naturally occurring ions and free electrons within the gas. As their kinetic energy approaches the binding

energy, they start ionizing and dissociating the gas molecules, at which point there is said to be plasma breakdown. As they and their electrons continue accelerating (heating up) and ionizing other particles, which are then also accelerated from the induced loop voltage, the electrons cascade to eventually form a highly ionized plasma. Consequently, the loop voltage induces a current with the charged plasma gas particles. This plasma has a toroidal current due to the magnetic field of the transformer coil. The current and a vertical magnetic field help provide a needed equilibrium field for the plasma. Without the current, the vertical field would not be able to counter the outward expansion forces on the plasma. The current has the additional effect of producing a poloidal magnetic field, which helps provide stability.

Since the induced current relies upon a changing current in the transformer, this form of power is inherently limited. Even worse, as the plasma heats up, the resistance decreases, and so the heating power generated by the current will saturate. Fortunately, there are several other ways to provide plasma heating. Radio frequency waves can be used to heat the plasma beyond the temperature which the Ohmic transformer reaches. Energetic beams of neutral particles can also be injected to heat the plasma in a process also known as Neutral Beam Injection, or NBI.

The ion temperature is an important characteristic of the plasma because the fusion reaction rate is a strong function of temperature, and most fusion is predicted to come from the energetic ions, particularly the higher energy ions. Auxiliary heating methods can enhance this by generating an ion tail. The ion tail is comprised of the particles at the high end of the energy distribution which exceed the normal Maxwellian distribution. The temperature is also important for determination of the efficiency of the various auxiliary heating methods. The temperature gradient is important to heat flux, and hence to the confinement time of energy as well.

The Alcator C-Mod Tokamak [1] is a high magnetic field, high density fusion

experiment, with advanced magnetic shaping. Alcator C-Mod has a major radius of 66 cm, and a minor radius of 21 cm. Alcator C-Mod also has a divertor to study divertor physics. It is a closed type divertor, which can be filled with gas to simulate a radiative type of divertor as well. Fueling is provided by gas puffing and pellet injections. Typical C-Mod toroidal magnetic field strengths are around 5 Tesla, though future runs are expected to reach 9 Tesla on axis. Typical plasma currents have been as high as 1 MegaAmpere, but can reach as high as 3 MA with the higher Toroidal field.

In addition to the Ohmic heating of the plasma, Ion Cyclotron Radio Frequency heating can also be applied. During the 1993 campaign, a TiC coated movable single strap (monopole) antenna was used for RF heating experiments on port D. For the 1994 campaign, a TiC coated fixed two-strap (out of phase operation) dipole antenna replaced the monopole antenna on port D for RF experiments. Up to 1.8 MW of power has been coupled into the plasma with a power density of about 10 MW/m^2. A second antenna with a Boron-Carbide (B_4C) coated Faraday shield will also be used with a 2 MW transmitter at 80 MHz on port E.

The charge exchange neutral particle analyzer measures the flux of neutral particles which leave the plasma. The neutral particles are formed through a charge exchange collision in which a fast ion picks up a neutral particle's electron. This can be used to measure the ion velocity distribution function, $f(v_i)$, so heating effects can be investigated. This measurement is especially useful in showing the effects of Ion Cyclotron Radio Frequency heating upon the high energy ions. The charge exchange analyzer will also provide the Maxwellian ion temperature.

Since several CX analyzers could look at different R/R_0 angles, the resonance layer could also be explored during ICRF shots. A scanning CX analyzer could also be employed for this purpose for several repeated shots if the plasma conditions can be reproduced from shot to shot. The temperature given by the CX analyzer can also be compared to other ion temperature measurement diagnostics, such

as HIREX, which measures Argon line width broadening, and the global neutron emission detectors which use the fusion rate and fusion cross section's temperature variation to determine the plasma temperature. This is often a helpful comparison in experiments.

In this thesis, the range of parameters in which the Charge Exchange Neutral Particle Analyzer (CX analyzer) can be expected to yield sensible data will be explored. The particular CX analyzers considered are used on the Alcator C-Mod tokamak. Charge exchange analysis does have limitations in its range of operation. The plasma conditions, notably ion density and temperature, for the particles to undergo charge exchange events, and escape the plasma without further charge exchange so that they can be detected, are limited. High ion densities can make the plasma opaque to neutral particles, and hence limit the CX analyzer to looking at the edge of the plasma. At high plasma temperatures the CX cross section decreases rapidly and ionizing collisions start to dominate, so again the core of the plasma becomes opaque to CX neutrals. The analyzer is also limited in terms of detector saturation. Stray neutrons (from D-D fusion) and photons (hard x-rays and gamma rays) can raise the level of background noise in the detectors to the point where the the actual data is hidden. The results section of this analysis will show the predicted ranges of the plasma conditions for the CX analyzers to operate.

Chapter 2

Background Physics

A plasma is composed of energetic electrons and ions. Typically, they are in a Maxwellian velocity distribution about a particular velocity, which corresponds to an energy referred to as the temperature. The velocity distribution is considered to have an energetic "tail" when it is heated, where the tail is a non-thermal distribution which is added to the Maxwellian, as shown in Figure 2-1. Neutral particles are also present in the plasma, with a higher density near the edge of the plasma where the temperature is lower, and fewer ionizing events occur due to lower cross sections for ionizing events. A typical Alcator C-Mod plasma electron density and temperature profile is shown in Figure 2-2. A typical profile of ion temperature is shown in Figure 2-3. The neutral density profile is calculated using the FRANTIC code. FPPRF also uses this code to determine the neutral density profile, so Figure 2-4 is included from the output of FPPRF.

The types of collisions that are important to this analysis include charge exchange collisions, ionizing collisions with ions, and ionizing collisions with electrons. Charge exchange collisions occur when the atomic electron is captured by the ion. A description of this process can be found in Reference [2]. This involves a quantum resonant transfer of the electron. As such, the cross section increases as the time

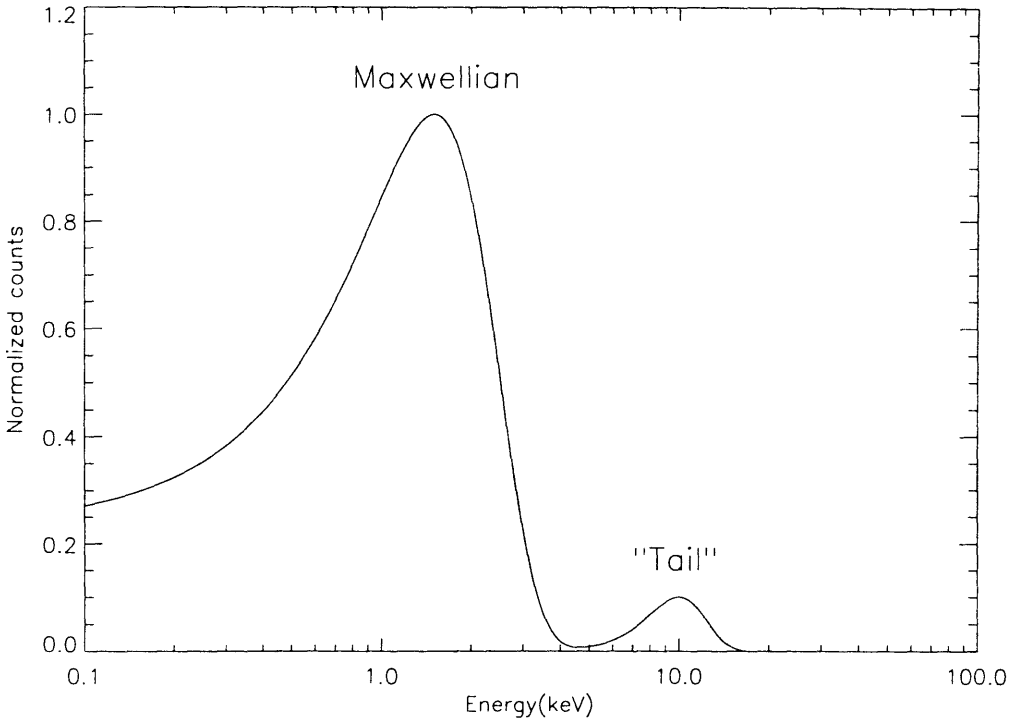

Figure 2-1: Maxwellian Distribution with Tail

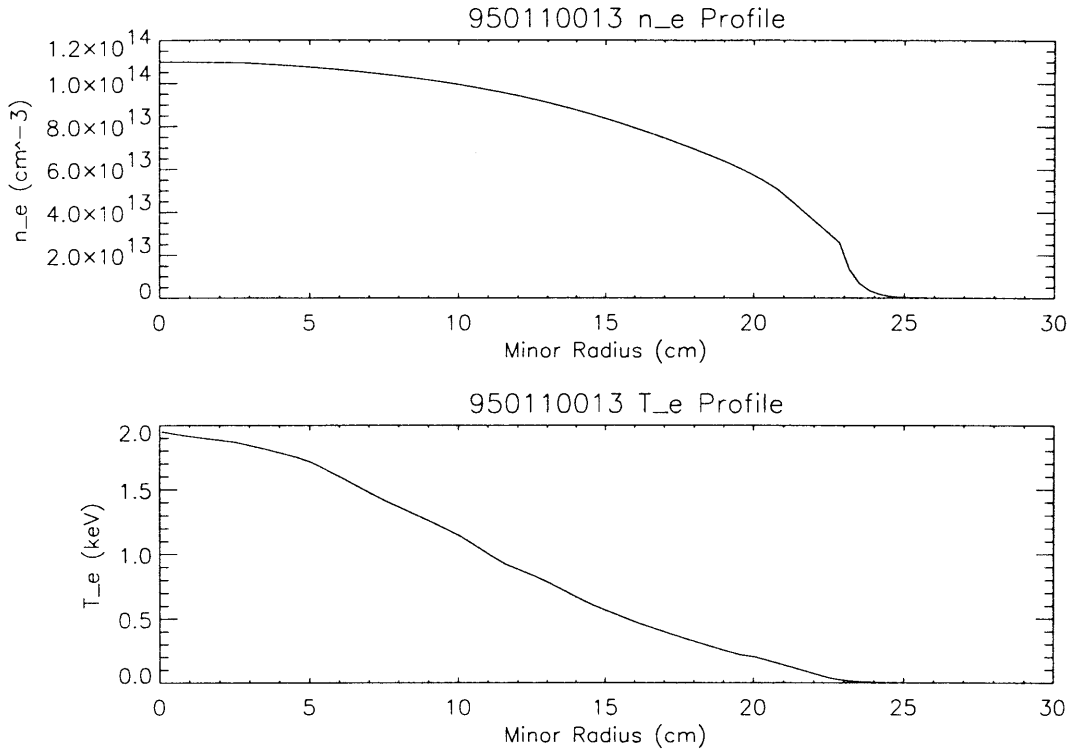

Figure 2-2: Typical Electron Profiles

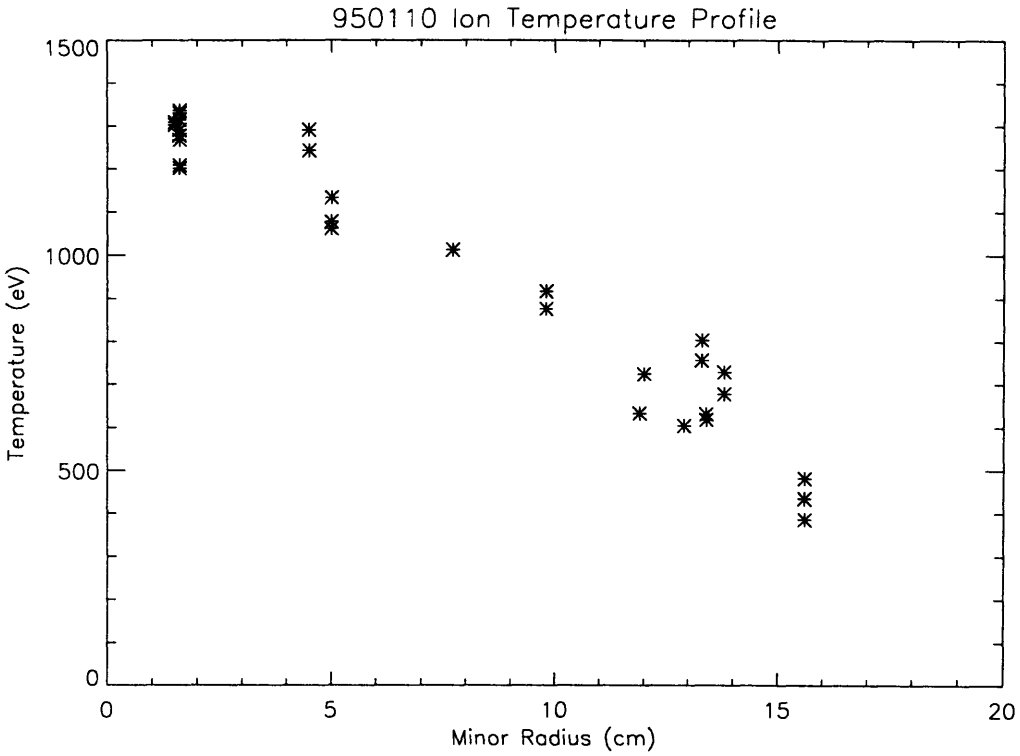

Figure 2-3: Typical Ion Temperature Profile (from HIREX)

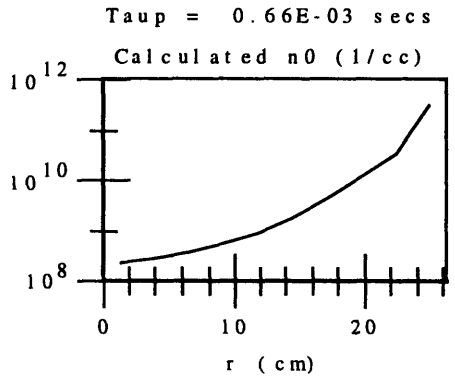

2 FPP/SPRUCE 30-JAN-95 17:31:03 USER10:[MILLER.RUNFPP]CX05_05.IN;3

Figure 2-4: Typical Neutral Density Profile

which the nuclei are close increases. When the ion's relative velocity exceeds the electron orbital velocity (the Rydberg energy divided by the ratio of the ion mass to the electron mass is: $R_y \frac{m_i}{m_e} \approx 20\ keV$) the translational effect breaks the resonance.

As competitive mechanisms, ionizing collisions attenuate the charge exchange neutral flux. To determine the probability of a charge exchange neutral leaving the plasma, one must consider the energy dependence of the various collisions. The cross sections of these events are shown in Figure 2-5 (taken from [4], but originally produced in [5]). Since the electrons typically move with a much higher velocity than the neutral particles, the atom can be considered as stationary in the ionizing collisions with electrons until the energy of the atom exceeds that of the electron by $m_i/m_e(\approx 1800)$. The electron ionization process has a threshold energy, R_y, below which the cross section is zero. Ionizing collisions with ions are similar to ionizing collisions with electrons, except that the energy of the ion must be m_i/m_e higher than that of an electron for ionization to occur. However, the low electron mass allows the ionizing electron's path to be deflected more than the ionizing ion's, especially at the lower energies near the threshold, so the cross sectional dependence is not exactly the same.

The Charge Exchange Neutral Particle Analyzer works by being able to detect ions which have undergone a single charge exchange event. This event does not affect the energy of the particles involved more than a few eV, so the now neutral ion will have essentially the same energy which it possessed prior to the collision. For the particle to reach the analyzer, it must not undergo another charge exchange collision nor an ionizing collision.

The now neutral particles will then travel in a straight path in the direction of their motion after the charge exchange event. By limiting the solid angle of the analyzer line of sight, the path the neutral particle beam takes to reach the analyzer can be well defined. This results in the ability to measure a line integral of the charge exchange flux. If multiple analyzers are used, the line integrals can be

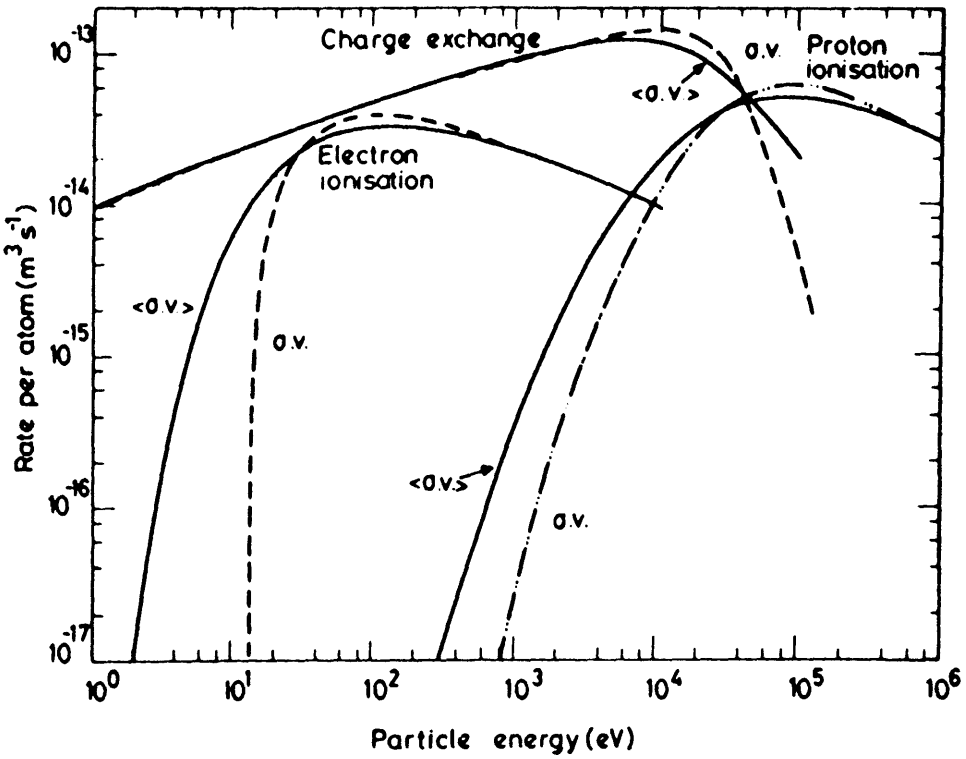

Figure 2-5: Collisional Cross Sections

unfolded to show the spatial distribution of the temperature.

The analyzer uses a stripping cell to strip off the electrons which the neutral particles have picked up via charge exchange in the plasma, when they were ions. The stripping cell contains a relatively high density of neutral molecules, which is Helium at about $10^{12} - 10^{13}\ cm^{-3}$ to optimize the stripping efficiency for the analyzers used on Alcator C-Mod. The electrons of those atoms collide with the charge exchange neutral particles' electrons to ionize the energetic atoms. The analyzer then uses a magnetic field to separate the ion beam by their energies and also to separate the ions from the unstripped neutral particles. The ions travel along a gyroradius determined by their velocity perpendicular to the magnetic field and the magnetic field strength by the $\vec{v} \times \vec{B}$ force. An electric field parallel to the magnetic field also separates the ionized portion of the beam by mass at the same time, allowing detectors to measure the number of particles of a given mass and energy, as shown in Figure 2-6.

2.1 Calculation of $\vec{E}$ and $\vec{B}$

As mentioned above, the magnetic field separates the ions according to their energy. This is through the magnetic portion of the Lorentz force, the velocity crossed with the magnetic field. Since this is a cross product, it does not affect the energy of the particles, only their direction. For a uniform magnetic field, this produces a circular path with a well defined gyroradius.

The electric field is chosen to be parallel to the magnetic field so that the force on the ions only accelerates them parallel to the magnetic field and thus does not alter the gyroradial behavior of the ions in the direction perpendicular to the magnetic field. The electric field will accelerate the ions with a force of qE and give them an acceleration proportional to qE/m. Since this depends upon the ratio

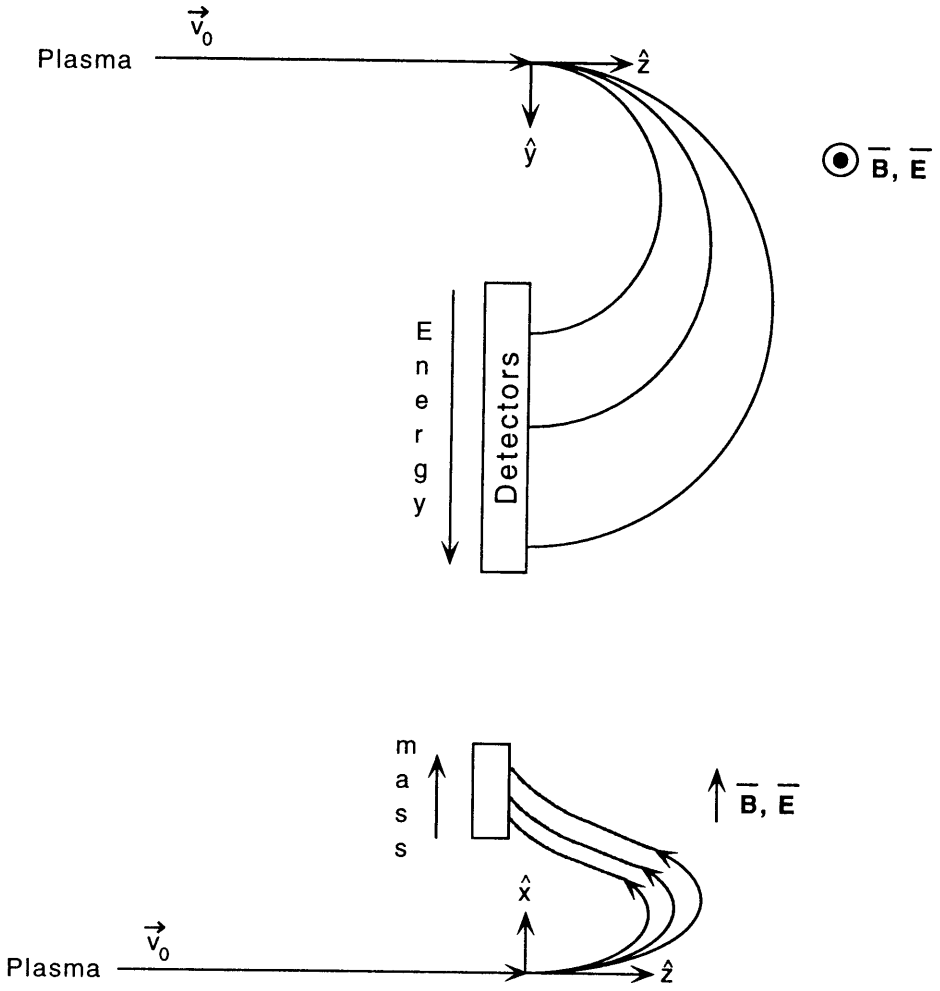

Figure 2-6: Particle Orbits

of the charge of the ions to their mass, this will separate isotopes of a particular species. Since the electric field is parallel to the magnetic field, $v_\perp$ is constant, and this increase in energy will not affect the effect which the magnetic field has upon the particles.

To calculate the fields needed to separate the particle beam according to mass and energy, the forces on the particles are taken into consideration. To simplify the analysis, the coordinates are carefully chosen and some simplifying assumptions are made. Figure 2-6 shows a simple schematic of the problem.

Assuming :

(i) $\vec{v_0} = v_{z0}\hat{z}$ $\qquad K_p = \frac{1}{2}mv_0^2$

(ii) $\vec{B} = B\hat{x}$ $\qquad$ Constant in space and time.

(iii) $\vec{E} = E\hat{x}$ $\qquad$ Constant in space and time.

(iv) Non-relativistic particles

(v) Negligible collisions inside the analyzer

The electromagnetic forces on the particles are from the magnet and electrostatic field plates in the analyzer.

$$\vec{F} = q(\vec{E} + \vec{v} \times \vec{B}) = qE\hat{x} + qv_zB\hat{y} - v_yqB\hat{z}$$

From Newton's Law, $F_y = m\frac{dv_y}{dt} = v_zqB$

and $F_z = m\frac{dv_z}{dt} = -v_yqB$

But, since $v_z = \frac{m}{qB}\frac{dv_y}{dt}$, then $m\frac{dv_z}{dt} = m\frac{d}{dt}(\frac{m}{qB}\frac{dv_y}{dt}) = \frac{m^2}{qB}\frac{d^2v_y}{dt^2}$

Rearranging this, $\frac{m^2}{(qB)^2}\frac{d^2v_y}{dt^2} + v_y = 0$

The solution to this is simply $v_y = C_1\ cos(wt) + C_2\ sin(wt)$ where $w = \frac{qB}{m}$

The Larmor radius will be $R_c = \frac{v_\perp}{w} = \frac{mv_\perp}{B}$, where $v = \sqrt{\frac{2K_p}{m}}$ and $v_\perp = v_0$ from the initial conditions.

From the diagram, our boundary conditions are:

$v_y(t=0) = 0 \qquad \Rightarrow C_1 = 0$

and $v_y(wt = \frac{\pi}{2}) = -v_{z0} \qquad \Rightarrow C_2 = v_{z0}$

Then $v_y = -v_{z0}\ sin(wt)$

$v_z = v_{z0}\ cos(wt)$

The final distance travelled will be $y_f = 2R_c = 2c\sqrt{\frac{2K_p}{mc^2}} \times \frac{m}{qB}$, $(R_c = \frac{\sqrt{2K_p m}}{qB})$.

$B = 2c\sqrt{\frac{2K_p}{mc^2}} \times \frac{m}{qy_f} = 6 \times 10^8 \sqrt{K_p(keV)m(amu)}\sqrt{\frac{2(1000)}{938\times10^6}}\ \frac{1.673\times10^{-27}}{qy_f(cm)\times1.6022\times10^{19}}$

To get the magnetic field strength required for particles of a given energy, K_{max}, to go to a channel at a certain distance, y_f, the formula for the magnetic field is:

$$B(Tesla) = 0.915\ \frac{\sqrt{K_p(keV)m(amu)}}{qy_f(cm)} \tag{2.1}$$

Now that B is determined, the energy associated with the first channel can be determined. Holding B constant in Equation 2.1, the dependence of energy and position can be used to determine the energy of the first channel to the energy of the last.

$$B(Tesla) = 0.915\ \frac{\sqrt{K_{p\ min}m}}{qy_{min}} = 0.915\ \frac{\sqrt{K_{p\ max}m}}{qy_{max}}$$

$$K_{p\ min} = (0.915)^2\ \frac{K_{p\ max} m (q y_{min})^2}{(0.915)^2 m (q y_{max})^2} = \frac{K_{p\ max} y_{min}^2}{y_{max}^2}$$

In fact, for each channel i,

$$K_{p\ i} = (0.915)^2\ \frac{K_{p\ max} m (q y_i)^2}{(0.915)^2 m (q y_{max})^2} = \frac{K_{p\ max} y_i^2}{y_{max}^2}$$

Now for motion in the $\hat{x}$ direction, once again Newton's Law is invoked,

$F_x = m\frac{dv_x}{dt} = qE$

Simple integration yields:

$$v_x = \frac{qE}{m}t \tag{2.2}$$

And again, to solve for x, $x = \frac{qE}{2m}t^2$.

Knowing that the particle will travel half of an orbit in the z-y plane, that the speed is constant at v_{z0}, and that the distance traveled is $\pi R_c = v_{z0}\, t_f$, we can solve for t_f.

$$t_f = \frac{\pi R_c}{c}\sqrt{\frac{mc^2}{2K_p}} \tag{2.3}$$

So then,

$$x_f = \frac{qE}{2m}\left(\frac{\pi y_f\sqrt{m}}{\sqrt{8K_p}}\right) = \frac{qE(\pi y_f)^2}{16K_p}$$

$$E = \frac{x_f 16K_p}{q\pi^2 y_f^2} \tag{2.4}$$

Converting to more useful units, we get:

$$E(V/m) = \frac{(0.01)x_f 16K_p(1.602\times10^{-19})}{q\pi^2(0.01)^2y_f^2(1.673\times10^{-27})} = 1621\frac{x_f K_p}{qy_f}$$

Or, in kV/cm,

$$E(kV/cm) = 1.621\frac{x_f(cm)K_p(keV)}{qy_f^2(cm)} \tag{2.5}$$

Some typical numbers for the analyzer may be $y_f = 50\ cm$, $x_f = 2\ cm$, an electrostatic plate $gap = 5.5\ cm$, $K_p = 100\ keV$, and looking at Hydrogen, $m = 1$, and $q = 1$.

Then $B(kG) = 0.915\ \frac{\sqrt{(100)(1)}}{(1)(50)} = 0.183$ kG.

$E(kV/cm) = 1.621\ \frac{(2)(100)}{(1)(50)^2} = 0.130$ kV/cm, and $V = (0.130)(5.5) = 713$ volts.

As a side note, the relationship between E and B can be found. From Equation 2.3, solve with R_c in terms of B.

$$t_f = \frac{\pi R_c}{c}\sqrt{\frac{mc^2}{2K_p}} = \frac{\pi\sqrt{2K_p m}}{qB}\sqrt{\frac{mc^2}{2K_p}} = \frac{\pi m}{qB}$$

$$x_f = \frac{qE}{2m}(\frac{\pi m}{qB})^2 = \frac{Em\pi^2}{2qB^2}$$

$$\frac{E}{B^2} = \frac{2qx_f}{m\pi^2} = constant \tag{2.6}$$

2.2 Unfolding the flux

To determine the plasma temperature from the flux that reaches the detectors, various corrections must be taken into account. From the plasma's distribution, the CX cross section's energy dependence produces an energy distribution of neutral flux. Other considerations include the solid angle, attenuation along the beam line, and the stripping cell efficiency, which also have an energy dependence.

To unfold these effects, start at the plasma and incorporate them into the flux calculation. In the plasma, the rate of charge exchange per unit volume is:

$$R = \frac{dn_0}{dt} = \int d^3\vec{v_i} \int d^3\vec{v_0} f_i f_0 \sigma_{cx}(v_i - v_0)$$

Assuming a Maxwellian ion distribution, and a Dirac delta function as the neutral distribution, then

$$f_i = \frac{n_i \exp(\frac{mv_i^2}{2T_i})}{(2\pi\frac{T_i}{m})^{\frac{3}{2}}} \text{ and } f_0 = \frac{n_0\delta^3(\vec{v}-\vec{v_0})}{4\pi v_0^2}$$

Where $n_i = \int f_i d^3\vec{v_i}$ and $n_0 = \int f_0 d^3\vec{v_0}$

For the isotropic case, and assuming $T_0 \approx 0$, $d^3\vec{v_i} = 4\pi v_i^2 dv_i$ and $d^3\vec{v_0} = 4\pi v_0^2 dv_0$.

Assuming non-relativistic particles, $v_i = \sqrt{\frac{2K_p}{m_i}}$ therefore, $dv_i = \sqrt{\frac{1}{2mK_p}} dK_p$.

$$d^3v_i = \frac{8\pi}{m}\sqrt{\frac{K_p}{2m}} dK_p$$

So finally,

$$\frac{dn_0}{dt} = \int \frac{\sigma_{cx} v_i n_i n_0 \exp(-\frac{mv_i^2}{2T_i}) d^3v_i}{(\frac{2\pi T_i}{m})^{\frac{3}{2}}}$$

Since $\frac{dn_0}{dt}$ is important for each channel and not the whole energy range, $\triangle K_{channel}$ is small and $\sigma_{cx}(K)$, $v\sqrt{K}\exp(-\frac{K}{T_i})$ can be considered to vary slowly enough over the integral for each channel to be taken as constants. Then, for each channel j,

$$[\frac{dn_0}{dt}]_j = \sigma_{cx} v_i \sqrt{K_j} \exp(-\frac{K_j}{T_i}) \frac{8\pi}{\sqrt{2}} \frac{n_i n_0}{(\frac{2\pi K T_i}{m})^{\frac{3}{2}}} \int dK_j$$

To get the neutral flux, Γ_0 , multiply by the solid angle, Ω_a, of the apertures as seen by the plasma and an effective plasma area seen by the apertures, A_p. Then apply an attenuation coefficient, $\eta(l)$, along the path length, l, to determine the neutral flux to the detector, Γ_0.

$\Omega_a = a/R^2$, where a is the aperture area, and R is the distance from the plasma to the aperture.

$A_p = \Omega_2 R^2$, where Ω_2 is the solid angle of the plasma seen by the apertures, and R is the distance to the plasma.

For each channel, j, $\int dK_j$ is $\triangle K_j$,

$$\Gamma = \frac{2\Omega_a A_p}{\sqrt{\pi}} \int dl\ \eta(l)\ n_i(l)\ n_0(l)\ \sigma_{cx}(K_j)\ v_i\ \sqrt{K_j}\ \triangle K_j\ \frac{\exp(-\frac{K_j}{T_i})}{(T_i)^{\frac{3}{2}}}$$

The number of particles reaching the detectors, N, is related to the flux by:

$$\frac{dN}{dK_p} = \frac{1}{\sqrt{K_p}} \frac{d\Gamma}{dK_p}$$

Some additional simplifying approximations can be made at this point. If the charge exchange reaction coefficient, $\sigma_{cx} v_i$, varies slowly enough, then the average coefficient for the plasma at the ion temperature can be used, $< \sigma_{cx} v_i >$. The

energy dependent terms can be taken out of the path length integral, and the result is:

$$\frac{dN}{dK_p} = \frac{2A\Omega_a}{\sqrt{\pi}} < \sigma_{cx} v_i > \frac{\exp(-\frac{K_p}{T_i})}{(T_i)^{\frac{3}{2}}} \int \eta n_0 n_i dl$$

Rearranging the $< \sigma_{cx} v_i >$ term, and taking the natural log of both sides helps to separate out the energy dependent terms.

$$\ln(\frac{1}{< \sigma_{cx} v_i > \frac{dN}{dK_p}}) = \ln[\frac{2A\Omega_a}{\sqrt{\pi}} \int \eta n_0 n_i dl] - \frac{3}{2}\ln(T_i) - \frac{K_p}{T_i}$$

$$\frac{d}{dK_p}\ln(\frac{1}{< \sigma_{cx} v_i > \frac{dN}{dK_p}}) = -\frac{1}{T_i} = \frac{d}{dK_p}(\ln(\frac{dN}{dK_p}) - \ln(< \sigma_{cx} v_i >)) \qquad (2.7)$$

The actual cross section can then be used directly in equation 2.7, in conjunction with the count rate of the detectors to determine the temperature. For a count rate of N in a channel with an energy range of δK, and knowing the charge exchange reaction coefficient, $< \sigma_{cx} v_i >$, one gets the temperature by;

$$\frac{1}{T_i} = -\frac{d}{dK}[\ln(\frac{dN}{dK_p}) - \ln(< \sigma_{cx} v_i >)]$$

2.3 Resolution

The question now arises as to how precise the temperature measurement will be. To look at this problem, the resolution of particle energy and the mass rejection are examined.

The energy resolution can be determined by first looking at the range of energies each channel would see for a point source, then including the finite aperture sizes and the consequent smearing of energies that would accompany them.

Uncertainties are also present due to the measurement of the electric and magnetic fields, in distances, such as from the stripping cell to the plasma, and uncertainties concerning the stripping cell efficiency either from measurements of the stripping cell pressure or other mechanisms. Additional errors can be introduced through mis-alignment.

2.3.1 Energy resolution

For the theoretical model, one can easily calculate the energy range of a channel by simply calculating the energy of particles that will reach either end of the channel and calculating the difference. Starting with Equation 2.1, one gets the following.

$$B(Tesla) = 0.915\ \frac{\sqrt{K_{max}m}}{qy_f}$$

$$K = \frac{B^2q^2y^2}{(0.915)^2m} = (\frac{y}{y_f})^2K_{max}$$

$$\Delta K = K(y+\Delta y) - K(y-\Delta y) = \frac{(y+\Delta y)^2 - (y-\Delta y)^2}{y_f^2} K_{max}$$

$$\frac{\Delta K}{K} = \frac{(y+\Delta y)^2 - (y-\Delta y)^2}{y^2} = 4\frac{\Delta y}{y}$$

The actual aperture size smears the energies a channel will see. Assuming perfect alignment of the apertures, and that they are rectangular with dimensions of x_a and y_a separated by the stripping cell length, l_{sc}, an approximation of the energies viewed by each channel can be determined.

The upper portion of Figure 2-7 shows the diagram of this problem. The initial conditions for the two extremes will then be that $\vec{v_0} = v_{y0}\hat{y} + v_{z0}\hat{z}$ where $\alpha = tan^{-1}(\frac{y_a}{l_{sc}})$, $v_{y01} = v_0\ sin(\alpha) \approx v_0\ tan(\alpha)$, $v_{z01} = v_0\ cos(\alpha)$, $v_{y02} = -v_{y01}$, and $v_{z02} = v_{z01}$.

The particles still move with a gyroradius, but they do not travel exactly a half circle. Figure 2-7 shows the new paths the particles will travel. The new y_f for the extremes, y_{f1} and y_{f2} will be:

$$y_{f1} = 2cos(\alpha)R_c + tan(\alpha)(\frac{l_{sc}}{2} + l_{atomag}) = cos(\alpha)y_{f0} + (\frac{y_a}{2} + \frac{l_{atomag}y_a}{l_{sc}}) \qquad (2.8)$$

$$y_{f2} = 2cos(\alpha)R_c - tan(\alpha)(\frac{l_{sc}}{2} + l_{atomag})$$

One can now determine the range of energies which a channel will detect. The lower energy will be determined by particles which have an extra $tan(\alpha)(\frac{l_{sc}}{2}+l_{atomag})$

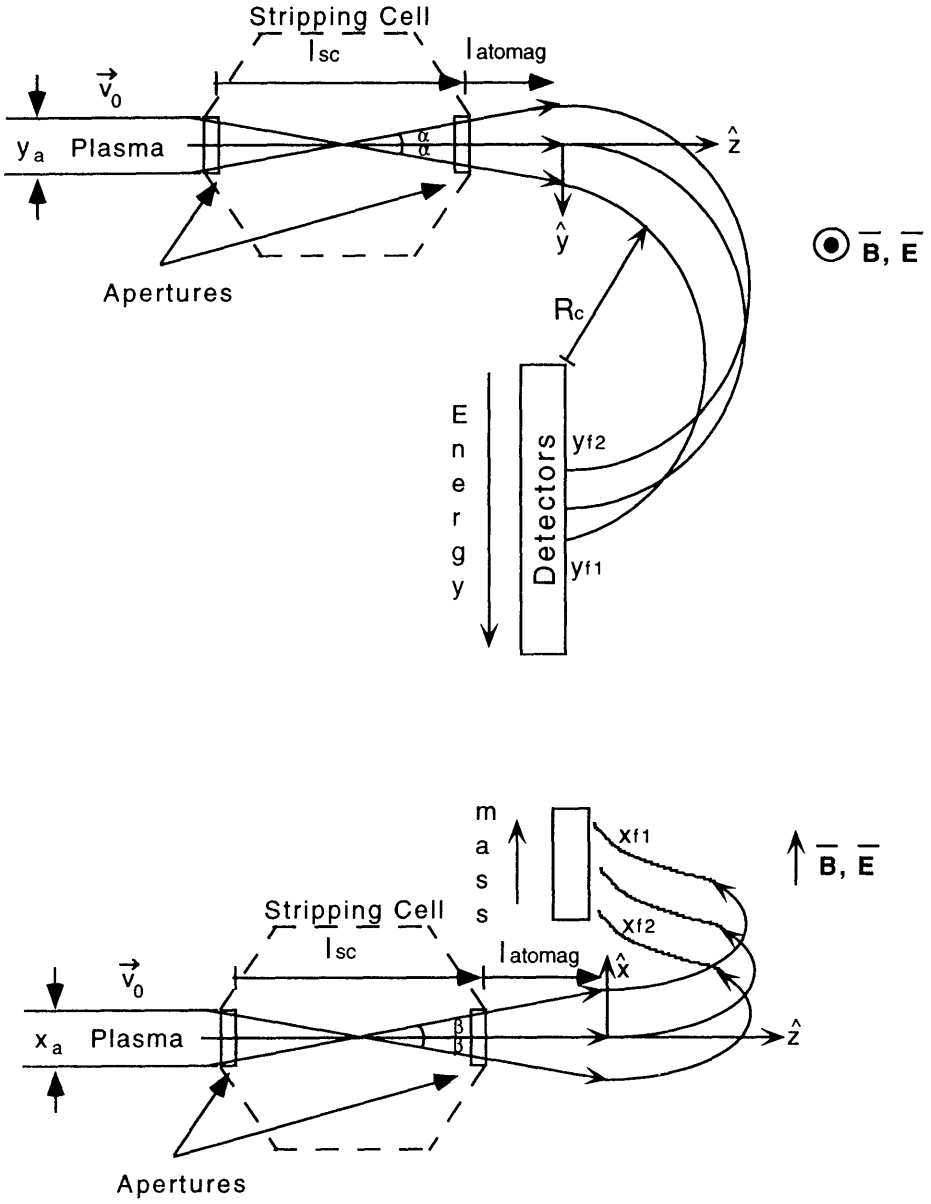

Figure 2-7: Finite aperture particle paths

added to their orbit, y_{-1}, while the higher energy particles will have that amount subtracted from their orbit, y_1. For a channel width of $2\Delta y$ about y_0, the range of energies is determined from the following derivation.

$$y_{f0} + \Delta y = y_{f1} - tan(\alpha)(\frac{l_{sc}}{2} + l_{a\ to\ mag})$$

$$y_{f1} = y_{f0} + \Delta y + tan(\alpha)(\frac{l_{sc}}{2} + l_{a\ to\ mag})$$

But $y_{f0} = \frac{\sqrt{Km}}{Bq}$, so this reduces to:

$$\frac{\sqrt{K_1 m}}{Bq} = \frac{\sqrt{K_0 m}}{Bq} + \Delta y + \frac{y_a}{l_{sc}}(\frac{l_{sc}}{2} + l_{a\ to\ mag})$$

$$\sqrt{K_1} = \sqrt{K_0} + (\frac{Bq}{\sqrt{m}})y_a(\frac{1}{2} + \frac{l_{a\ to\ mag}}{l_{sc}} + \frac{\Delta y}{y_a})$$

Defining $K_{off} = \sqrt{K_1} - \sqrt{K_0}$, a similar derivation shows that the lower energy, K_{-1} is found by:

$$\sqrt{K_{-1}} = \sqrt{K_0} - K_{off}$$

So then ΔK is simply:

$$\Delta K = K_1 - K_{-1} = K_0 + 2\sqrt{K_0}K_{off} + K_{off}^2 - [K_0 - 2\sqrt{K_0}K_{off} + K_{off}^2] = 4\sqrt{K_0}K_{off}$$

The resolution is:

$$\frac{\Delta K}{K} = \frac{4K_{off}}{\sqrt{K_0}} = \frac{4Bqy_a}{\sqrt{m}}(\frac{1}{2} + \frac{l_{atomag}}{l_{sc}} + \frac{\Delta y}{y_a}) \tag{2.9}$$

This can be used with the actual dimensions to determine each channel's energy resolution. This result is also helpful for the cross calibration derivation, shown in Section 4.2.

2.3.2 Mass Rejection

For the mass rejection, there will be an initial velocity in the direction of the electric field, as shown in the lower portion of Figure 2-7. This will alter the final position, x_f, into x_{f1} and x_{f2} for particles with an initial velocity in the direction with and against the acceleration, respectively. This initial velocity gets put into Equation 2.2 and the solution yields:

$$v_x = \frac{qE}{m}t + v_{x0} = \frac{dx}{dt}$$

$$x = \frac{qE}{2m}t^2 + v_{x0}t + x_0$$

From the lower portion of Figure 2-7,

$$\beta = tan^{-1}(\frac{x_a}{l_{sc}})$$

Since no forces act upon the particles until they pass into the analyzer main vacuum chamber,

$$x_0 = \pm(\frac{x_a}{2})(1 + \frac{l_{atomag}}{l_{sc}})$$

$$v_{x0} = \pm(\frac{x_a}{l_{sc}})v_{z0}$$

The time of flight is determined by the time it takes the particle to travel the gyroradius. Given the finite aperture sizes, this is no longer the simple form of before, but rather depends on the y offset from the straight path. Since the larger time of flight will yield the larger deviation, Equation 2.8 is used to calculate the time of flight.

$$t = \frac{\pi y_{f0}(1 + \frac{\alpha}{2\pi})}{2v_{z0}}$$

Since x is measured from the normal beam path, the range of x will be:

$$x = \frac{qE}{2m}t^2 + v_{x0}t + x_0$$

From Equation 2.4,

$$E = \frac{16x_{f0}K_p}{q\pi^2 y_{f0}^2} = \frac{8x_f m v_{z0}^2}{q\pi^2 y_{f0}^2}$$

Then,

$$x = \frac{qx_{f0}mv_{z0}^2}{2mq\pi^2 y_{f0}^2}[\frac{\pi y_{f0}(1 + \frac{\alpha}{2\pi})}{2v_{zo}}]^2 \pm \frac{x_a v_{z0}}{l_{sc}}\frac{\pi y_{f0}(1 + \frac{\alpha}{2\pi})}{2v_{zo}} \pm \frac{x_a}{2}(1 + \frac{l_{atomag}}{l_{sc}})$$

$$x = x_{f0}(1 + \frac{\alpha}{2\pi})^2 \pm \frac{\pi x_a y_{f0}(1 + \frac{\alpha}{2\pi})}{2l_{sc}} \pm \frac{x_a}{2}(1 + \frac{l_{atomag}}{l_{sc}}) \qquad (2.10)$$

Chapter 3

Hardware

Two types of charge exchange analyzers are used on Alcator C-Mod. Though each is of a different design, they share similar features. Both analyzers use an electric field parallel to a magnetic field to separate the particles according to their mass and energies. Each also has a stripping cell to ionize the charge exchange neutrals, a main chamber, where the magnets and electrostatic plates are located, and a set of detectors.

An older analyzer, designed for PDX (see also Reference [3]) but used on Alcator C-Mod, will look tangentially to the plasma at a R/R_0 of ≈ 1, and is referred to as the Tangential Charge eXchange analyzer, or TCX. The TCX analyzer is mass resolving and can observe either H ions to 40 keV or D ions to 20 keV with its 10 Channeltron detectors. When looking at 40 keV in H, the detector energy widths range from 0.32 keV at 4.04 keV in channel 1 to 2.0 keV at 40 keV in channel 10.

A second charge exchange analyzer, referred to as the Perpendicular Charge eXchange analyzer, or PCX, can scan horizontally from $R/R_0 = 0.0$ (perpendicular to the plasma) to $R/R_0 = 0.72$ (13°). It can also scan vertically from 0° to 13°. The

PCX analyzer uses 39 energy columns for each of 2 mass rows to simultaneously resolve the energy distributions of H and D ions at energies up to 600 keV and 300 keV respectively. When looking at 600 keV H ions, channel 1 has an energy width of 6.5 keV around 37.9 keV, and channel 39 has a width of 25.7 keV about 600 keV. The arrangement of the analyzers on Alcator C-Mod is shown in Figure 3-1.

3.1 TCX Hardware

The TCX analyzer uses an electric field parallel to a magnetic field to physically separate various ionic species from within a beam of such particles, as shown in Figure 2-6. The main components of the analyzer are shown in Figure 3-2, and include the stripping cell, the electric field plate, the magnetic poles, the detectors, and the vacuum system. Since there is only one row of detectors, the TCX analyzer can only look at one ion species at a time. The TCX analyzer can detect particles up to 40 keV in H, and 20 keV in D.

The TCX magnetic poles are mounted on the top and bottom lids of the main analyzer vacuum chamber with the windings outside the vacuum. The gap between the poles is 1 cm, and they provide a nominal field of 4 kGauss at 12 Amperes of current. The main chamber vacuum walls are made of 2.5 cm thick soft iron to both provide a return path for the magnetic flux and to shield the chamber from stray magnetic fields, such as those generated within the tokamak.

The TCX electrostatic field plate is a trapezoidal plate 3.5 cm above a ground plate which is parallel to the electrostatic plate and the bottom magnet face. It is also slightly lower than the magnet face. The shape of the electrostatic plate is designed so that the time of flight of the ions is constant for all 10 channels. This keeps the vertical displacement a function of only mass, and not energy.

The stripping cell of the TCX analyzer is 15 cm long, and is optimally operated in He around 0.5 mTorr (N_2 equivalent). At either end of the stripping cell are mounted a series of 5 apertures. The outermost apertures are 0.23 cm in diameter. These reduce scattering and improve the mass resolution. The pressure in the box outside the stripping cell is around 5×10^{-6} Torr (N_2 equivalent). The stripping cell efficiency is calculated (cf. Reference [6]) using the cross sections for charge

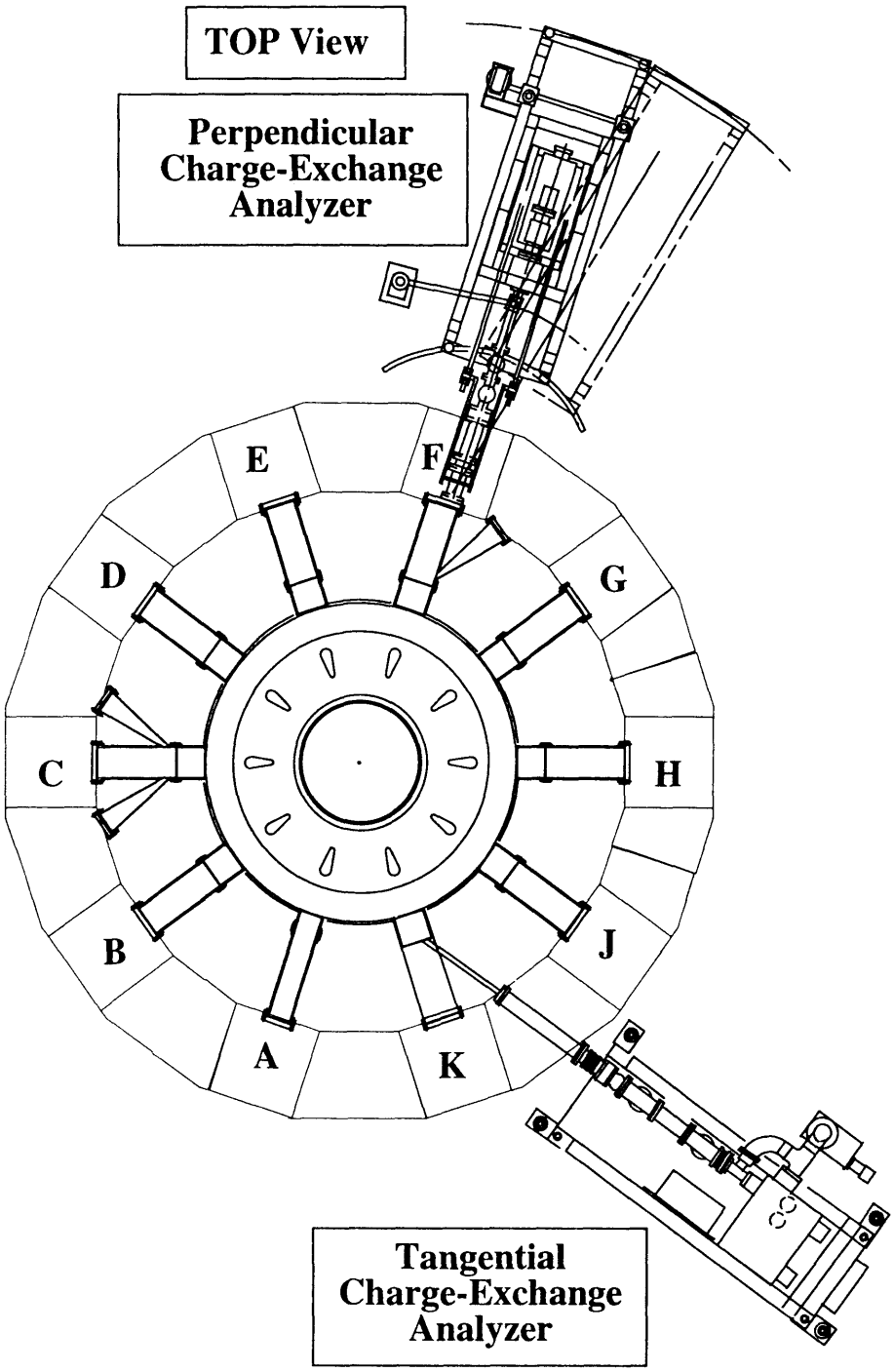

Figure 3-1: Alcator C-Mod layout

transfer (σ_{01} and σ_{10}), the scattering cross section, σ_s, an effective length (l_{eff}) times the stripping cell pressure, P, in Equation 3.1, which follows. An experiment at PPPL [7] verified the theory for the TCX analyzer. The energy dependence of the stripping efficiency, ε_s, for several stripping cell pressures is shown in Figure 3-3.

$$\varepsilon_s = \frac{\sigma_{01}}{\sigma_{01} + \sigma_{10}} \exp(-l_{eff} P C_1 \sigma_s) \times \{1 - \exp[(-l_{eff} P C_1 (\sigma_{01} + \sigma_{10})]\} \qquad (3.1)$$

Where $C_1 = 3.243 \times 10^{13} cm^{-3} mtorr^{-1}$ (at T = 25° C).

The TCX analyzer has 10 Channeltron electron multipliers (Galileo Electro-Optics Corporation Model 4830) to detect the ions in a pulse counting mode. The Channeltrons are operated at -3 kV, which is shielded from the main chamber by a transparent mesh. This mesh also improves detection uniformity. Between the high energy end of the magnet region and the electrostatic plates a baffle has been added to prevent energetic particles from reflecting off the ceramic support of the electrostatic plates. A schematic of the TCX analyzer is shown in Figure 3-2. From this, one can see the stripping cell, the magnet region, the electric field plates, and the detectors.

The TCX analyzer is limited in the range of particle energies it can view to about 40 keV for hydrogen. It can also only look at one species at a time, so it can only determine the minority ratio if a series of shots are repeated under the same conditions. A second analyzer, the PCX analyzer, was designed to allow a larger range of energies to be viewed, and to allow different species to be viewed simultaneously.

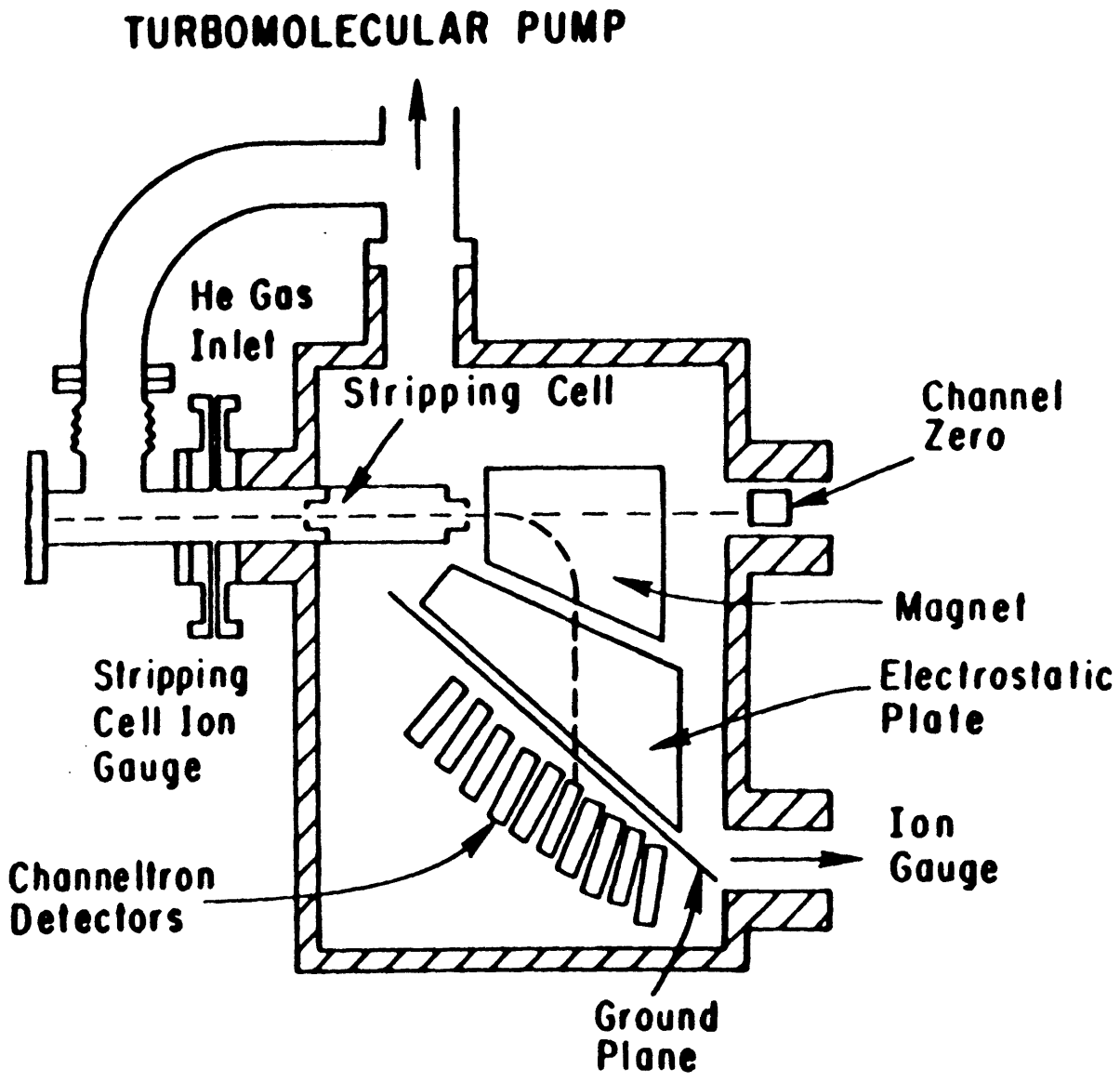

Figure 3-2: TCX Analyzer

3.2 PCX Hardware

The PCX analyzer has previously been used at Princeton's Plasma Physics Laboratory [8] to determine the velocity distribution of the plasma ions and the effects of heating by NBI and RF heating. A diagram of this analyzer is shown in Figure 3-4. It also uses an electric field parallel to a magnetic field to physically separate various ionic species from within a beam of such particles, as shown in Figure 2-6. The analyzer was originally designed to look at three ion species simultaneously, H^+, D^+, and T^+. With a typical set of operating parameters, the maximum energy of a hydrogen particle which the analyzer can detect can be determined from Equation 2.1. Taking the analyzer magnetic field at 4.2 kGauss, and the last channel 54 cm from the beam entrance,

$$K_{max}(keV, H) = \frac{B^2 q_H^2 y_f^2}{(9.15)^2 m_H} = \frac{(4.2)^2(1)^2(54)^2}{(9.15)^2(1)} \approx 600\ keV$$

The maximum energy of another ion, X, which the analyzer can detect will then be proportional to $\frac{m_H}{m_X} K_H$. This means that the PCX analyzer can look at energies up to 600 keV for H, 300 keV in D, and 200 keV in T, However, tritium ion densities are not expected to be high enough for detection in Alcator C-Mod, so only the lower two rows, for hydrogen and deuterium, of MCP channels are connected.

The main vacuum chamber of the PCX analyzer is 86.4 cm long by 54.9 cm wide by 16.51 cm deep. Its walls are 3.18 cm thick soft iron, which provides a return leg for the magnetic flux, as well as shielding the inside from stray magnetic fields. The positioning and spacing of the various components in the main vacuum chamber is shown in Figure 3-5.

The stripping cell is 24.8 cm in length, and 2.54 cm in diameter. It has apertures on either end which are rectangular slits, 0.24 cm by 0.13 cm. Typical operat-

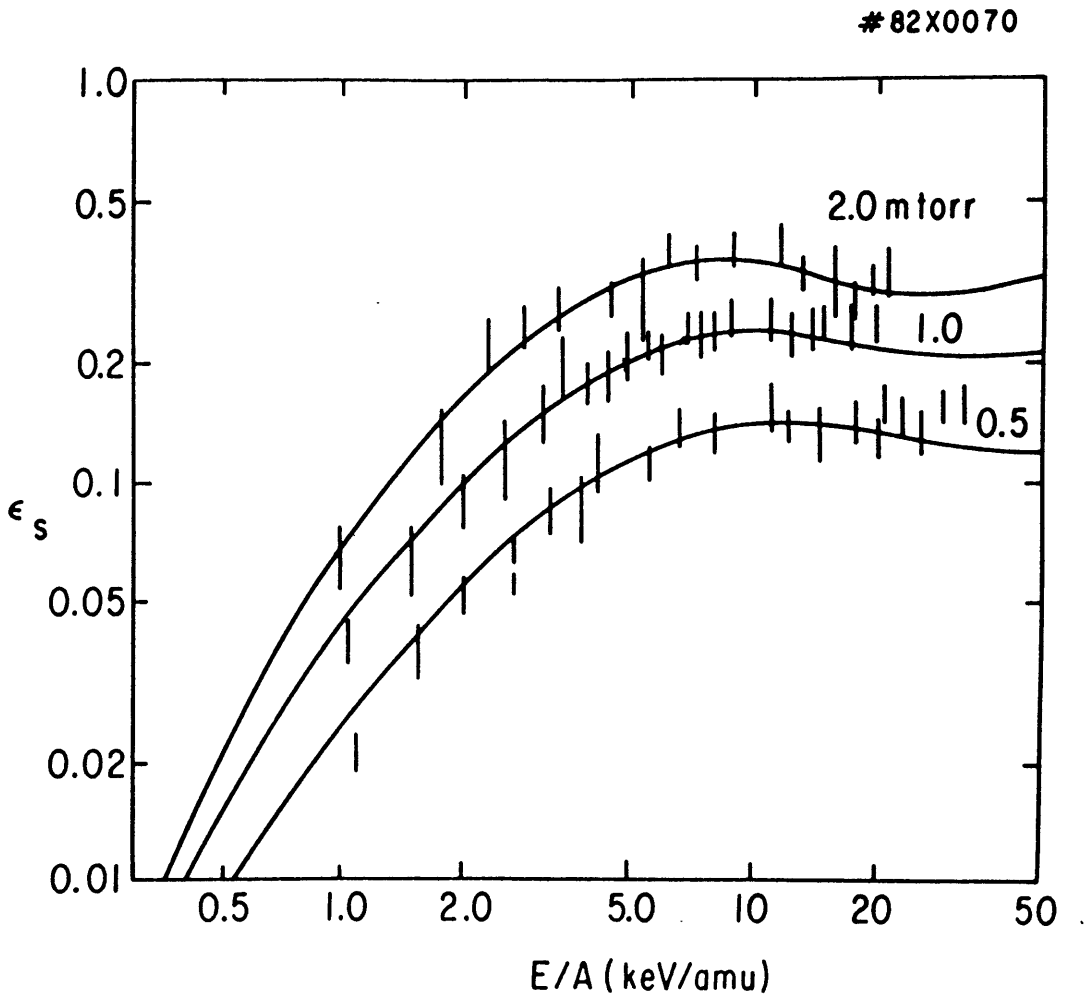

Figure 3-3: Stripping Cell Efficiency

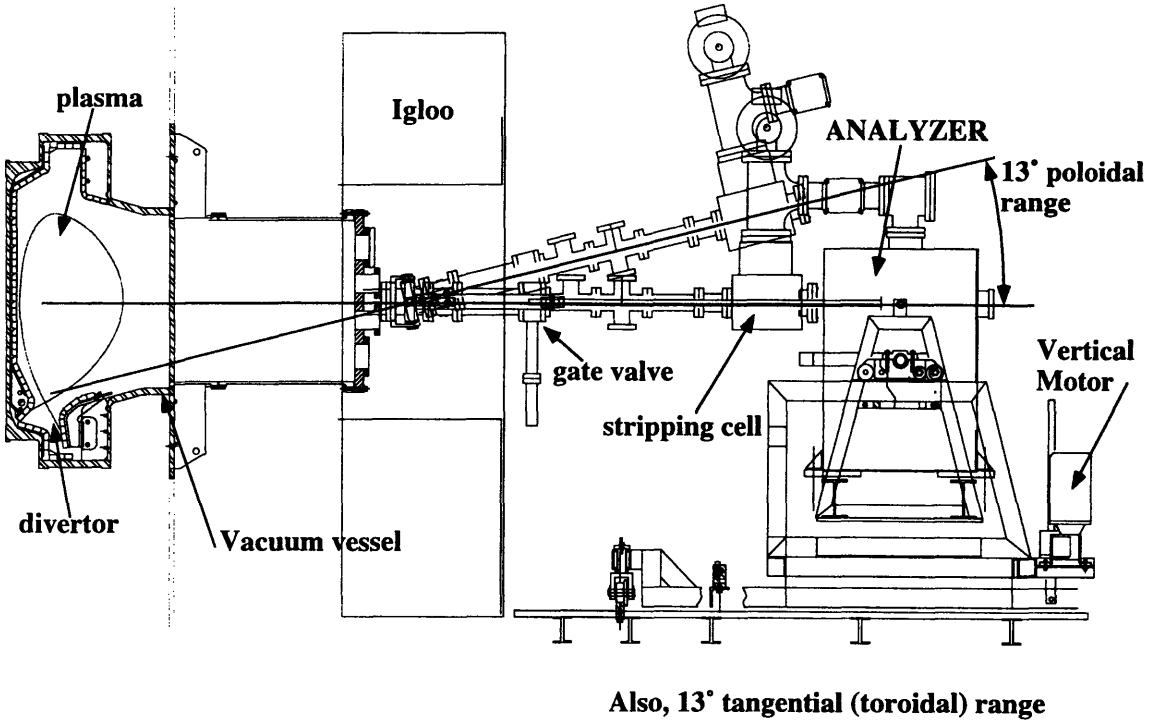

Figure 3-4: PCX Analyzer Components.

ing pressures are on the order of 1 mTorr (N_2 equivalent) in helium. The stripping cell is situated 245 cm from the plasma magnetic axis, as shown in Figure 3-8. The stripping cell efficiency is a function of the particle energies and stripping cell pressure, as mentioned in section 3.1 (cf. Figure 3-3).

It is now possible to calculate some of the important numbers from Chapter 2. Namely, y_i, x_1, x_2, and Ω_a, can now be determined.

From Figure 3-5, the distance, y_{max}, from the beam to the farthest MCP can be determined. From Figure 3-6, the distance from the far edge of the MCPs and the closest pin is 0.447 cm. The pin is 0.084 cm thick, so to the center of the pin is 0.405 cm. However, the pins are offset from the channel center by 2 mm, so the distance from the beam to the farthest channel is:

$$y_{max} = y_{39} = 86.36 - 20.003 + 2.540 - 6.35 - 8.604 - 0.405 + 0.20\ cm = 53.74\ cm.$$

The distance from the edge of the MCPs farthest from the beam to the nearest edge is 41.12 cm, and from the near edge to the closest pin is 0.52 cm. So the distance from the beam to the closest pin channel center is:

$$y_{min} = y_1 = 53.94 - 41.12 + 0.52 - \frac{1}{2}(0.084) + 0.20\ cm = 13.50\ cm.$$

The distance from the first channel of the first energy group to the first channel of the center energy group, y_{14}, is the length of the energy sections, 13.00 cm, plus the length of the gap between the energy sections, 1.092 cm. Then the distance from the beam to y_{14} is:

$$y_{center} = y_{14} = 13.50 + 13.00 + 1.09 = 27.59\ cm.$$

From these reference points, the other channels' y-coordinates can be determined since the distance between adjacent channels in an energy group is 1.0 cm.

The distances from the beam to the mass rows can also be calculated from Figures 3-5 and 3-6.

$$x_1 = 3.81 + 4.366 + 2.654 - \frac{1}{2}(0.183) - 3.175 - 5.080 - 1.27\ cm = 1.21\ cm$$

$$x_2 = x_1 + 1.331 + 0.183 = 2.73\ cm$$

$$x_3 = x_1 + 3.137 - \frac{1}{2}(0.084) - \frac{1}{2}(0.183) = 4.22\ cm$$

The solid angle, Ω_a, can be calculated from the sizes of the apertures and the distances between them. To ensure that they determine the limiting solid angle, the solid angles defined by the baffle openings will also be calculated.

First, from the stripping cell apertures, which are expected to be the most limiting, the solid angle is:

$$\Omega_a = \frac{x_a y_a}{l_{sc}^2} = \frac{(0.24)(0.13)}{24.8^2} = 5.1 \times 10^{-5}$$

For baffles 1 and 2, the nozzle, and the snubber, the area is half the diameter squared times π.

$$\Omega_{b1} = \frac{\pi(\frac{d_1}{2})^2}{l_1} = \frac{\pi(\frac{2.223}{2})^2}{147.4^2} = 1.4 \times 10^{-4}$$

$$\Omega_{b2} = \frac{\pi(\frac{d_2}{2})^2}{l_2} = \frac{\pi(\frac{1.91}{2})^2}{101^2} = 2.8 \times 10^{-4}$$

$$\Omega_{nozzle} = \frac{\pi(\frac{d_{noz}}{2})^2}{l_{noz}} = \frac{\pi(\frac{0.723}{2})^2}{(24.8+14.3)^2} = 2.7 \times 10^{-4}$$

$$\Omega_{snubber} = \frac{\pi(\frac{d_{snub}}{2})^2}{l_{snub}} = \frac{\pi(\frac{0.794}{2})^2}{(24.8+14.9)^2} = 3.1 \times 10^{-4}$$

The important distances from the point the beam enters the main vacuum chamber to keep in mind are the minimum distance that a beam of like particles will take in the "x" direction, $x_1 = 1.21$ cm, the distance for the middle mass row, $x_2 = 2.73$ cm, and the farthest mass row, $x_3 = 4.22$ cm. In the "y" direction, $y_{min} = 13.50$ cm, $y_{max} = 53.74$ cm, and $\Omega_a = 5.1 \times 10^{-5}$.

The PCX electrostatic field plate (EP) is a "D" shaped metal sheet with a radius of 30.0 cm. The length of the edge is 60 cm, and the plate is 0.16 cm thick. This is separated from the magnet by a 0.08 cm thick piece of G-10 insulator, also in a "D" shape. The electric field plate power supply typically charges the plate to a few hundred volts, but can produce as much as 3 kV potential. The EP voltage

power supply provides an output signal for both the plate voltage and the current. This is used to determine the electric field produced by the EPs.

The PCX magnetic field power supply can generate up to 250 DC amperes. This can produce a magnetic field of around 5 kGauss, as shown in Figure 3-7. The magnet resistance at room temperature is about 250 $m\Omega$. The magnet is a "D" shaped coil with an 29.9 cm inner radius. The conductor consists of an 8x9 array of copper tubes. The tubes are 0.48 cm square, with a 0.23 cm diameter hole inside them. These tubes are separated from each other with a coated fiberglass insulator. The gap between the electrostatic field plate and its ground is 5.715 cm. The magnet power supply produces an output signal that measures the magnet current. This is used with a Gauss probe to determine the analyzer's magnetic field.

The PCX uses microchannel plate detectors (MCPs). They allow electron multiplication factors of $10^4 - 10^7$ with a resolution on the order of 100 picoseconds. Since the analyzer is only interested in resolving to 1 millisecond, this is more than adequate. To attain the higher multiplication factors, the MCPs are kept at high voltage, about 1 kiloVolt. Detection efficiencies in the 2-50 keV range for positive ions is reported to be 60-85% [10]. A diagram of the MCPs is shown in Figure 3-6. The voltage and current provided to each section (A, B, and C) of the MCPs is measured to monitor the voltage supplied to the detectors.

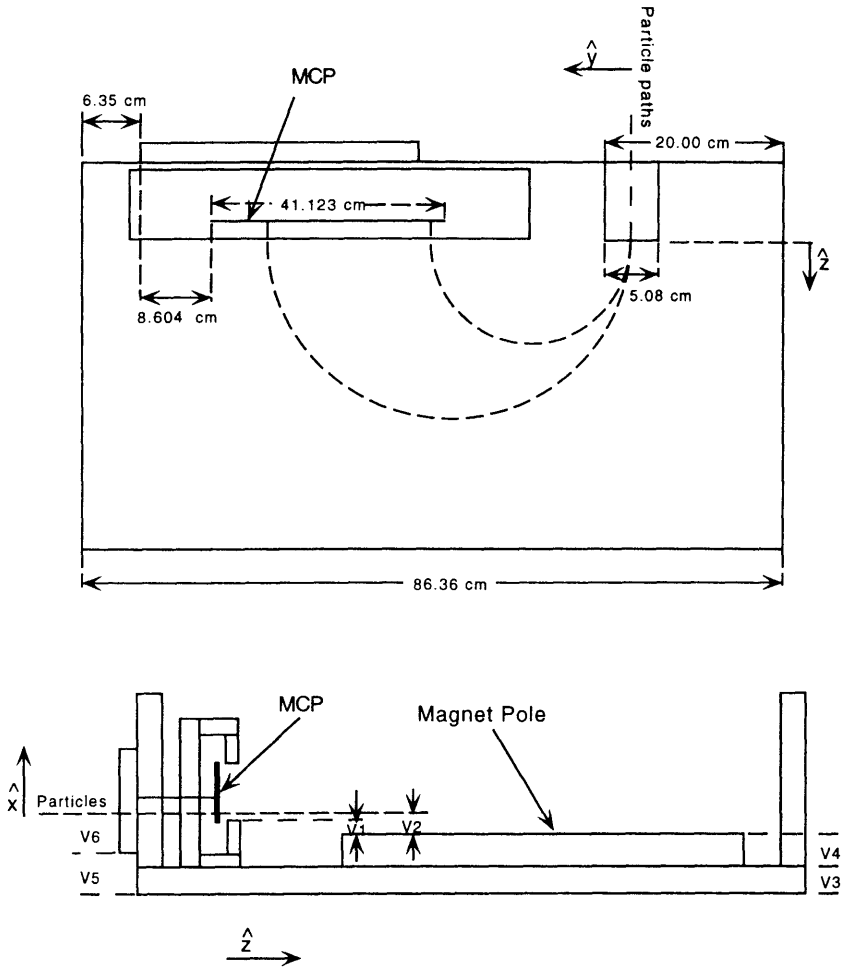

V1 = 0.79375 cm
V2 = 1.27 cm
V3 = 3.175 cm
V4 = 5.08 cm
V5 = 3.81 cm
V6 = 4.366 cm

Figure 3-5: PCX Main Vacuum Chamber

The EP and MCPs are kept in a vacuum with a pressure of $\leq 5 \times 10^{-6}$ Torr (N_2 equivalent) to prevent arcing. A turbo pump maintains this pressure in the detector chamber, while a smaller turbo pump maintains the beamline pressure. It is important to have a low beamline pressure for several reasons. The beamline pressure should be lower than the tokamak vacuum chamber pressure so that the beamline gas will not flow into the tokamak. Beamline gas also attenuates the neutral particles through various collisional mechanisms, so to get a high signal, the beamline should be kept at low pressure. To help keep this pressure low, a set of baffles were affixed to the plasma end of the beamline. One pair of baffles have a 1.9 cm diameter hole, and the other pair has a 2.2 cm diameter hole. The set with the larger hole is closer to the plasma, as shown in Figure 3-8.

The PCX analyzer is also capable of changing its poloidal or toroidal angle of sight between plasma shots. Two separate motors control the directions of motion. The poloidal angle is only changed when the toroidal angle is perpendicular. Similarly, the toroidal angle is only changed when the poloidal angle is at the midplane. Although this may seem to somewhat limit the capabilities of the analyzer, off angle sightlines would not yield useful results because of the asymetries involved. The position of the analyzer is measured with two position transducers, one for each direction (poloidal and toroidal).

With the actual PCX distances, the magnetic and electric fields required to look at energies ranging up to K_{max} for H in the lower row can be determined by using these distances in equations 2.1 and 2.5.

$$B(kGauss) = 9.15\frac{\sqrt{K_{max}(keV,H)m(amu)}}{qy_f(cm)} \qquad (2.1)$$

$y_f = 53.74$ cm

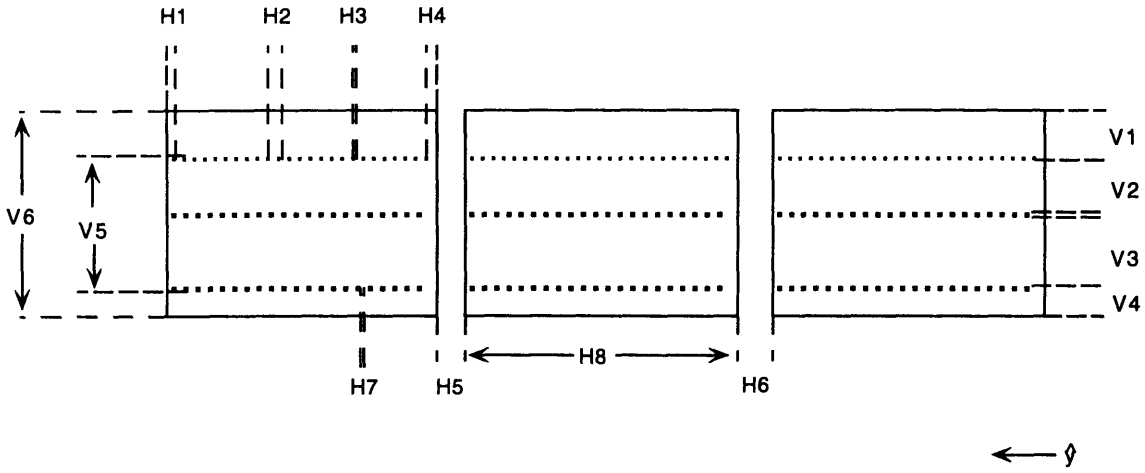

H1 = 0.447 cm
H2 = 0.574 cm
H3 = 0.084 cm
H4 = 0.523 cm
H5 = 1.024 cm
H6 = 1.092 cm
H7 = 0.183 cm
H8 = 13.00 cm

V1 = 2.595 cm
V2 = 1.382 cm
V3 = 1.331 cm
V4 = 2.654 cm
V5 = 3.137 cm
V6 = 8.148 cm

* Note, pins are offset 0.2 cm to the -$\hat{y}$ side of the actual channel centers.

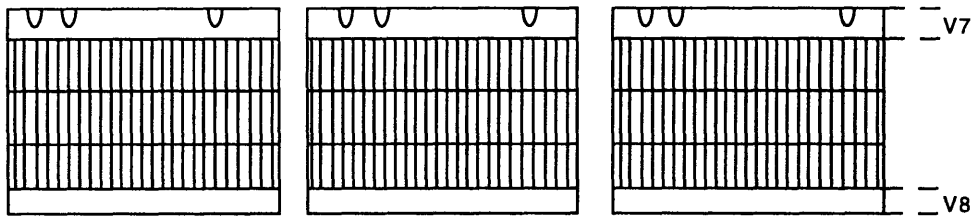

V7 = 1.92 cm
V8 = 1.92 cm

Figure 3-6: MCP detail

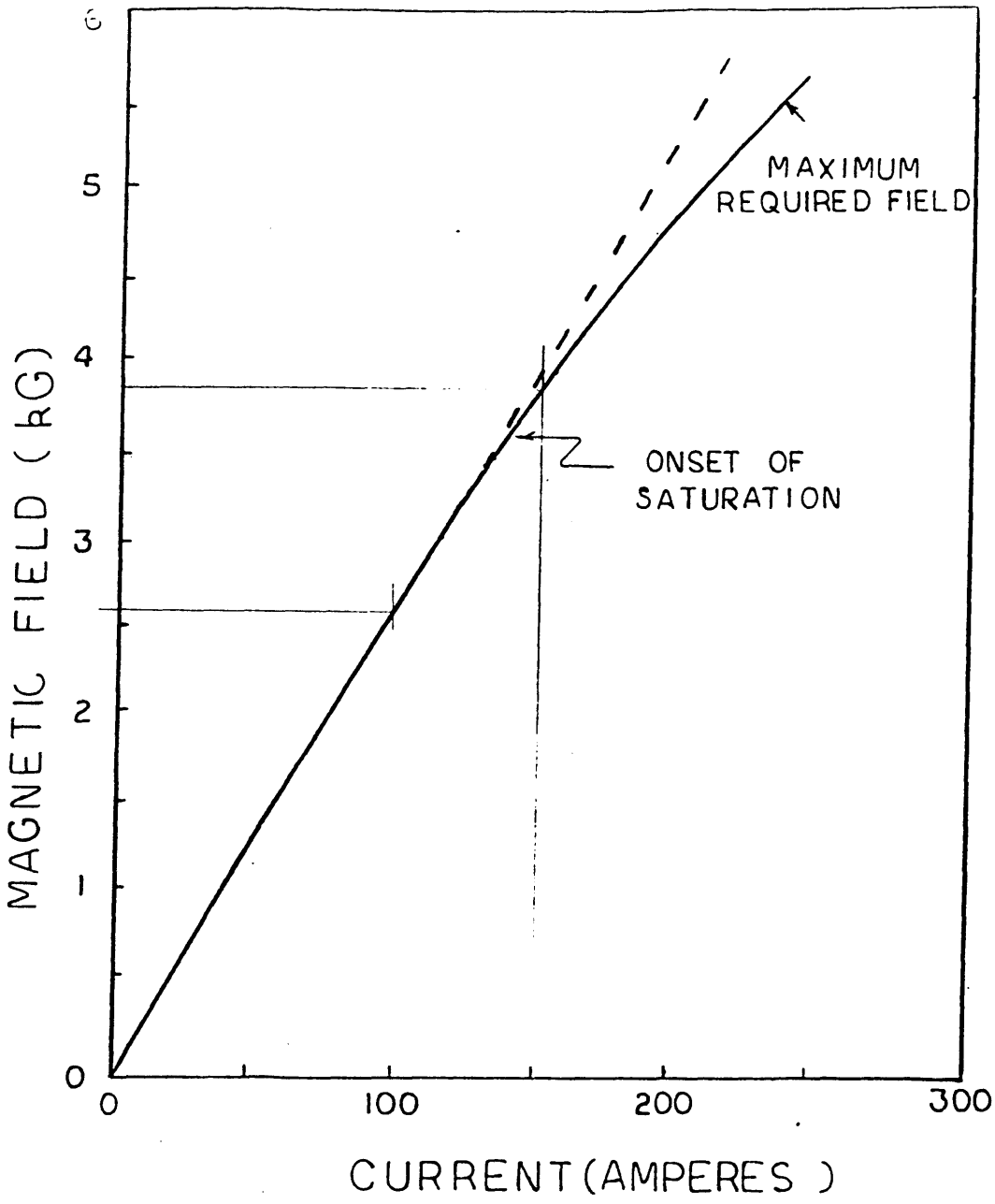

Figure 3-7: Magnet Current versus Field

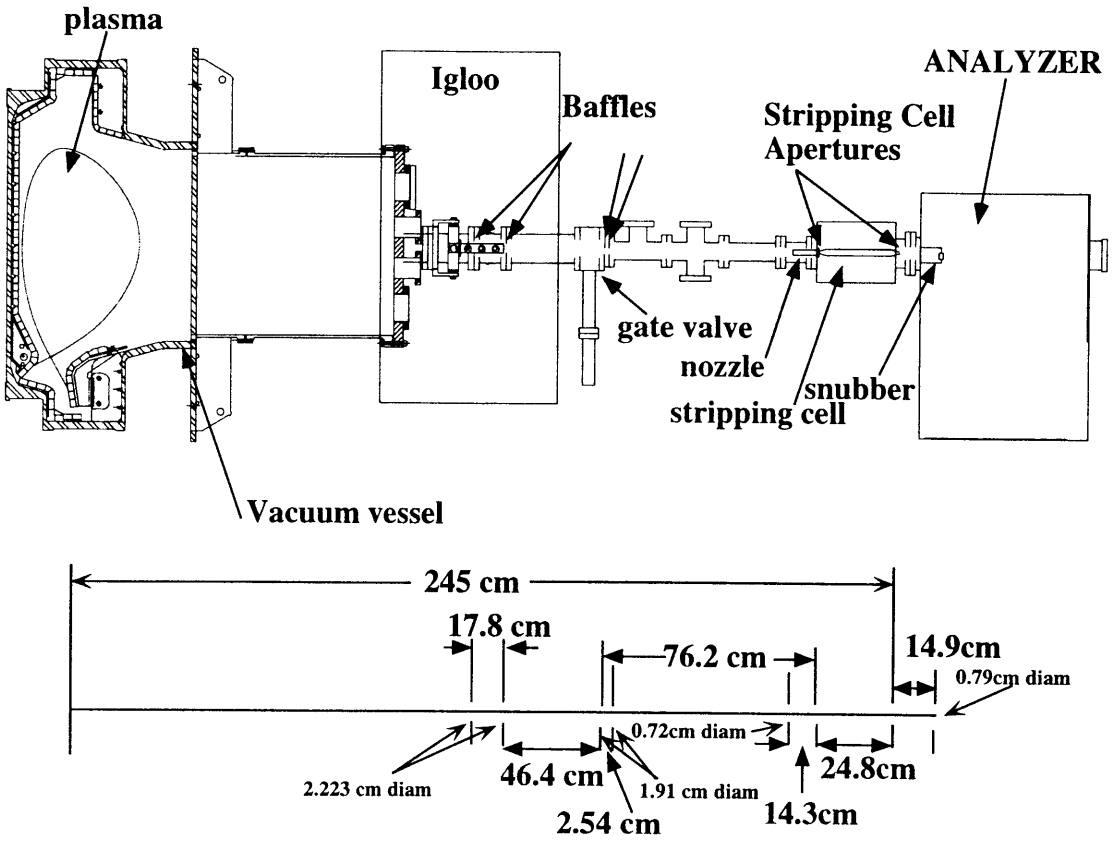

Figure 3-8: PCX Beamline

$q = 1$

$m = 1$

$$B(kGauss) = 9.15\frac{\sqrt{K_{max}(1)}}{(1)(53.74)} = 0.1703\sqrt{K_{max}(keV,H)} \tag{3.2}$$

The energy of the first channel for this magnetic field and the actual distances will then be:

$$K_{min} = \frac{K_{max}y_{min}^2}{y_{max}^2} = \frac{K_{max}(13.50)^2}{(53.74)^2} = 0.0631K_{max}$$

$$E(V/cm) = 1621\frac{x_f(cm)K_{max}(keV,H)}{qy_f^2} \qquad (Eq.\ 2.5)$$

$x_f = 1.21$ cm

$$E(V/cm) = 1621\frac{(1.21)K_{max}}{(1)(53.74)^2} = 0.679K_{max}(keV,H) \tag{3.3}$$

Since the gap between the electric field plate and its ground is 5.715 cm, then the voltage required is simply:

$$V(Volts) = E\ *\ gap\ = 0.679\ K_{max}(keV,H) * 5.715 = 3.88\ K_{max}(keV,H)$$

To the coordinates at which the deuterium particles will reach the MCPS, we go through the same calculations, but use m = 2 for the deuterium. y_f will be the same, as will the B and E fields. However, x_f will have to be recalculated, using Equation 2.1 as a starting point.

$$K_{max}(keV, D) = \frac{B^2(kG)q^2y_f^2(cm)}{(9.15)^2m(amu)} = \frac{(0.1703)^2K_{max}(H)(1)^2(53.74)^2}{(9.15)^2(2)} = 0.5K_{max}(H)$$

We can now calculate $x_f(D)$, using this value of $K_{max}(D)$, and m = 2.

$$x_f(D) = \frac{E(V/cm)qy_f^2(cm)}{K_{max}(keV, D)1621} = \frac{0.679K_{max}(H)(1)(53.74)^2}{0.5K_{max}(H)1621} = 2.42\ cm$$

Since we have measured $x_f = 2.73\ cm$, there might be cause for concern. However, the channels are 1.4 cm wide, so the second row's channels stretch from 2.03 cm $< x_f <$ 3.43 cm, and the beam will still be 0.4 cm within the channel.

For a $K_{max}(H)$ of 100 keV, $B(kG) = 0.1703\sqrt{K_{max}} = 1.7$ kG.

$E(V/cm) = 0.679\ K_{max} = 67.9$ V/cm, and $V = 5.715 * E(V/cm) = 388$ Volts.

The actual energy resolution of the channels can now be calculated as well. From Equations 2.9 and 2.1, $\frac{\Delta K}{K}$ can be calculated.

$$\frac{\Delta K}{K} = 4\frac{K_{off}}{\sqrt{K_0}} = \frac{4(\frac{Bq}{\sqrt{m}})[y_a(\frac{1}{2} + \frac{l_{a\ to\ mag}}{l_{sc}} + \frac{\Delta y}{y_a})]}{\frac{y_0 Bq}{\sqrt{m}}} \qquad (Eq.\ 2.9)$$

$\Delta y = 0.25$ cm

$y_a = 0.24$ cm

$l_{sc} = 24.8$ cm

$l_{a\ to\ mag} = 21.1$ cm

$$\frac{\Delta K}{K} = \frac{4[(0.24)(\frac{1}{2} + \frac{21.1}{24.8} + \frac{0.25}{0.24})]}{y_0} = \frac{2.30}{y_0}$$

For the closest channel, $y_0 = 13.50$ cm, so $\frac{\Delta K}{K} = \frac{2.30}{13.50} = 0.17$. For the farthest channel, $y_0 = 53.74$ cm, so $\frac{\Delta K}{K} = 0.043$.

The actual range in x with which the beam will strike the MCPs can be determined now as well. Starting with Equation 2.10,

$$x = x_{f0}(1 + \frac{\alpha}{2\pi})^2 \pm \frac{\pi x_a y_{f0}}{2l_{sc}}(1 + \frac{\alpha}{2\pi}) \pm \frac{x_a}{2}(\frac{l_{sc} + l_{atomag}}{l_{sc}}) \qquad (Eq.\ 2.10)$$

For mass row 1, $x_{fo} = 1.21$ cm.

$$x_1 = 1.21(1+\frac{tan^{-1}(0.24/24.8)}{2\pi})^2 \pm \frac{\pi(0.13)53.74}{2(24.8)}(1+\frac{tan^{-1}(0.24/24.8)}{2\pi}) \pm \frac{0.13}{2}(\frac{24.8+21.1}{24.8})$$

$$x_1 = 1.21 \pm 0.4425 \pm 0.120$$

So then 0.685 cm $\leq x_1 \leq$ 1.776 cm.

For mass row 2, $x_{fo} = 2.73$ cm.

$$x_2 = 2,73(1 + \frac{tan^{-1}(0.24/24.8)}{2\pi})^2 \pm 0.4425 \pm 0.120$$

So 1.865 cm $\leq x_2 \leq$ 2.99 cm.

Chapter 4

Calibration

The initial calibration of the CX analyzer was done at the Princeton Plasma Physics Laboratory. The procedure involved using ions from an accelerator to determine the analyzer response. The accelerator used for this experiment is a standard Cockroft-Walton accelerator, which can produce particles up to 150 keV. The ions used for the calibration had energies ranging up to about 60 keV, and the maximum energy scanned by the analyzer was 120 keV. The analyzer magnetic and electric fields were varied and the counting rates of the various Micro-Channel Plates were taken. The relative efficiency of each channel can be determined from these measurements. This data is then input into an IDL program that will unfold the raw data from the analyzer.

The second phase of calibration is a cross calibration of the MCP channels using the Alcator C-Mod plasma itself as an ion source.

4.1 Initial Calibration

At the Princeton Plasma Physics Laboratory, the initial calibration was performed as follows. Initially H_2^+ ions were used at around 15-30 keV with a magnetic field of approximately 2 kGauss to determine the relative efficiencies and set the gains to produce acceptable results. Then the electric field plate voltage, magnetic field, and ion beam energy were scanned to empirically determine the detector responses based upon the theoretical predictions.

The calibration procedure consisted of a series of runs. Each group of runs had a different set of MCP detectors connected to the Pre-Amplifying Discriminators (PADs). Within the groupings, different combinations of beam energy, magnetic field, and electric field were varied with small step-wise increases. Data was then collected for a set amount of time to measure the counting rate for the conditions at each step of the increase. A more detailed description will follow. A summary sheet of the runs is provided in Figures 4-1 and 4-2. The conventions for the tables are as follows:

The run header is indicated by the big bold letters in the top of the first column.

Section A is the section of MCPs closest to the beamline.

Section B is the middle section.

Section C is the section farthest from the beamline.

Mod refers to the run number for the group of runs.

Mass refers to the mass number of the channels being tested. Mass 1 is the closest to the beamline, mass 3 the farthest from it.

Spec refers to the ion species being used.

B(kG) is the magnetic field, in kGauss.

Ef(kV) refers to the electric field plate voltage. If the word 'vary' appears in this column, then the magnetic and electric fields were scanned together, according to Equation 2.6.

Eb (keV) refers to the beam energy, in keV.

Initially, the scalar counters were connected to the first two energy sections, A and B, of the lowest mass row, the mass 1 row. The data was saved under the file heading REJ-x-1-1, where the x is a counter for the run number. Run 5 had the magnetic field held constant at 0.78 kG and ion beam energy held at 37 keV while the electric field plate voltage was varied from 0 to 1.5 kV. This was used to fix the electric field and magnetic field at a particular ion beam energy. The count rates had a broad peak between 0.65 kV and 1.2 kV. An example of the data that this type of scan produced is shown in Figure 4-3.

For run 8b, the ion beam energy was varied while the magnetic field was held at 2.7 kGauss and the electric field plate voltage was held at 0.8 kV. An example of the data from one of the MCP channels for this type of scan is shown in Figure 4-4.

In run 9, the magnetic field and electric field plate voltage were varied (with $\frac{E}{B^2}$ held constant, as Equation 2.6 shows) with the ion beam energy held at 25 keV. This should move the beam across the anodes so that $\frac{E}{y^2}$ remains constant. The graph of this data is shown in Figure 4-5. This data was used to determine the relative calibration of the channels within the MCPs.

MIT	Mod	Mass	Spec	B (kG)	Ef (kV)	Eb (keV)	Comments
	4	1	1	1.55	220	10 - 50	about 5-6000 cts on straight through det
	5	1	1	0 - 2.5	0 - 1	25	
	6	1	1	1.55	0 - 1	25	Ch # 1 & 14 7 & 20 8 & 21
	7	1	1	1.55	0 - 1	30	
	8	1	1	0 - 2.2	vary	35	Egap to 5 cm in param file 3, #6 offset, #7 low eff
	9	1	1	0 - 2.2	vary	30	Changed PADs, #6 offset, #7 low eff still
							Changed PAD thresh to -10.5V(#6), -9.5V (#7)
							PAD back to -10V(#6), #7 not clean?
	11	1	1	scan	vary	30	No more #6 offset, #7 still low
	12	1	1	1	0.15	10 - 50	Thresh #7 set to -5V, better? Trouble with Ef ps
	13	1	1	1.55	0 - 1	31	Removed #15, put into #26 to check validity
	14	1	1	1.55	0 - 0.5	30.7	Ch #14 (Cicada) is #26 MCP again
Sec. C	15	1	1	scan	vary	20	Ch #7 is good, Ch #14 is still Ch #26 MCP
Sec. B	20	1	1	2	0.3	10 - 50	50 steps (#14 is #14) Not opt (7, 11, 12 dead)
PFC	Mod	Mass	Spec	B (kG)	Ef (kV)	Eb (keV)	Comments
Sec. B	1	1	1	2	0.24	8 - 50	ch. 7, 11, 12 dead (try thresh on 11 & 12 to -5V)
	2	1	1	2	0 - .6	20	ch #7 (Cicada) is #26 MCP
	3	1	1	2	0 - .6	20.5	ch 3&4 mixed, try to get 4 only
	4	1	1	scan	vary	25	ch #7 (Cic) is #26 MCP #11, 12 dead? Nice peak
	5	1	1	0 - 2.8	vary	35	34.5 panel, 35.8 mon. few random cts in 11 & 12
	6	1	1	0 - 2.8	vary	15	thresh 11 & 12 to -4V (Bf 100 amp com, 82 mon)
BOI	Mod	Mass	Spec	B (kG)	Ef (kV)	Eb (keV)	Comments
Sec. A	1	1	1	2	0.5	0 - 40	Ch 11, 12 offset (-5 V thresh) #7 -4V, new to -10V
	2	1	1	2	0-1	10	Ch 9 & 10 sat. Something after 1 kV?
	3	1	1	2	0-1.5	10	Reduced beam flux, too much
	4	1	1	2	0-1.5	10	reduced more #9 & 22 are fine
	5	1	1	0-3	vary	10	some saturated
	6	1	1	0-3.94	.01-1.4	10	lower flux, higher B to get 1 & 14, no 14?, no sat
	7	1	1	0-4.23	.01-1.6	9	Channel #26 MCP put in #7 Cicada
	8	1	1	3.02	1.24	10 - 50	ask 108 amp in mag mon 89.7, 26 MCP is 14 Cica
	9	1	1	2.51	1	10 - 50	not useful, no peaks, 91 ask, 74.4 mon, ch 26=14
	10	1	1	2.52	1.2	10 - 50	no good, too long count rates, more flux, ch 26=14

Figure 4-1: Initial Calibration Table of Runs(part 1)

REJ	Mod	Mass	Spec	B (kG)	Ef (kV)	Eb (keV)	Comments
A & B	1	1	1	0.78	0.4	10 - 50	no peak 14-25, SHV cable no go, same peak 1-13
bottom	2	1	1	1.61	0.4	10 - 50	SHV still bad, Problem with H2+ / broken
row	3	1	1	2.68	0.65	10 - 50	Ch 20, 24 dead (off), 25 replaced by 26, 12 by 13
	4	1	1	2.68	0 - 1	37.5	
	5	1	1	2.68	0 - 1.5	37	ch 14 broad peak 0.7-1.2 kV
	6	1	1	2.68	0.8	8 - 50	
	7	1	1	3.2	0.8	8 - 75	Should catch 1 & 25 Lower flux, energy pot not set
	8a	1	1	3.01	0.8	8 - 80	Problems with beam reproducibility
	8b	1	1	2.68	0.8	7 - 75	Final try, just missed #25
	9	1	1	0 - 2.8	0 - 0.7	10	
	10	1	1	0 - 3.5	0 - 1.3	25	
RLB	Mod	Mass	Spec	B (kG)	Ef (kV)	Eb (keV)	Comments
A & B	1	1?	1	2.67	0 - 2.5	37.5	ch 14 shows strong peak at > 1.5 kV, some quiet
mass	2	1?	1	2.66	1.7	7 - 80	1 keV diff panel/mon at 80 keV, ch 1 missed "half"
2 row	3	1?	1	0 -3.6	vary	25	field incorrect, try again
middle	4	2	1	0 - 3	vary	25	
	5	2	1	0 - 3.6	vary	25	try again, longer scan 0-130 amp asked ~3.6 kG
RBO	Mod	Mass	Spec	B (kG)	Ef (kV)	Eb (keV)	Comments
B & C	1	2	1	0 - 3.6	vary	35	MCP 26=1; d0, d1 = 1.15, Bf only to 100 amp ask
mass	2	2	1	1.5	1.7	0 - 70	nothing found
2 row	3	2	1	1.5	0 - 2	35	only 15 & 17 showed anything big near Ef = 0.5 kV
middle	4	2	1	1.5	0.5	7 - 70	
REB	Mod	Mass	Spec	B (kG)	Ef (kV)	Eb (keV)	Comments
B & C	1	1	1	1.5	0 - 1.5	35	MCP 26=1, peaks 0.15 to 0.35 kV in 15, 16, 17
mass 1	2	1	1	1.5	0.25	scan	
bottom	3	1	1	0 - 2.7	vary	35	d0=1, d1=1, but m=1

Figure 4-2: Initial Calibration Table of Runs(part 2)

The three types of scans were repeated for energy sections A and B in mass row 2 (RLB-x-2-1), B and C in mass row 1 (REB-x-1-1), and B and C mass row 2 (RBO-x-2-1).

The magnetic field was then calibrated by measuring the field with a Gauss probe, measuring the current through the magnets, and compared to the requested current. The ion beam energies were also measured and compared to the requested energy. The electric field plate voltages were also calibrated.

Figures 4-6 to 4-10 show the relative efficiencies determined for each of the constant beam energy runs. The different relative efficiencies were then normalized to each other by setting the relative efficiency of channel 42 (chosen because all of the runs had data at this point with reasonable counting rates) equal and then normalizing the result by the average relative efficiency. This is shown in Figures 4-11 and 4-12.

The roughness of the data can be attributed to several factors. The PADs were not always set to the proper thresholds. In addition, the electric field to magnetic field ratio, $\frac{E}{B^2}$, may not have been correct. In spite of these problems, the data was useful as a first guess of relative efficiencies and as a starting point from which correct magnetic and electric field strengths could be determined. However, it is clear that a more careful calibration should be performed. Hence the cross calibration (of the following section) was performed.

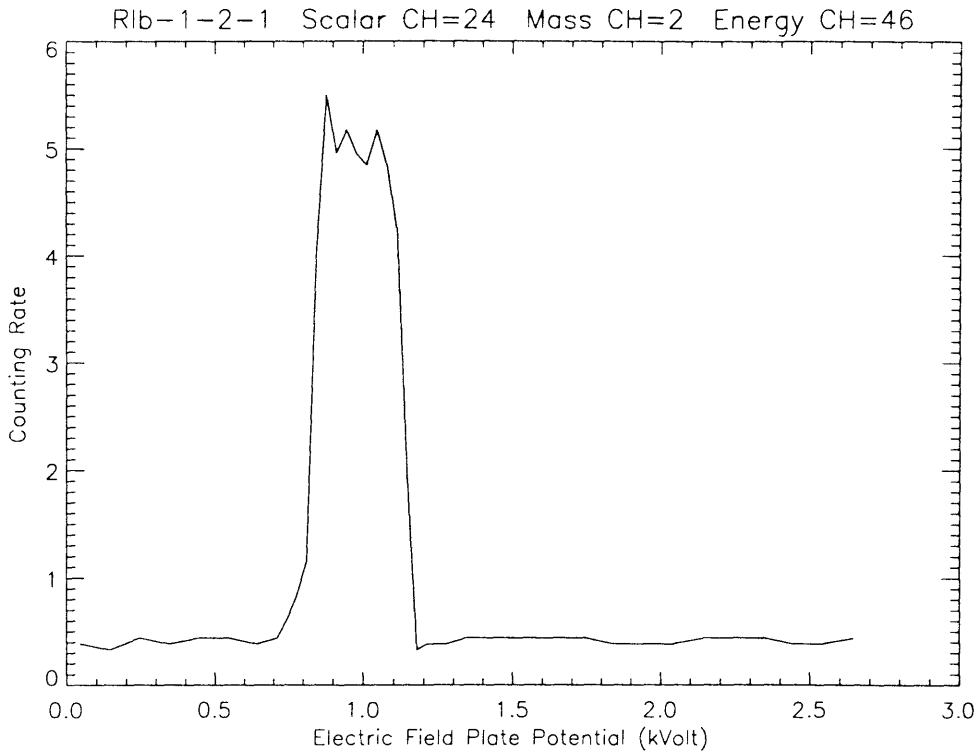

Figure 4-3: Electric Field Calibration

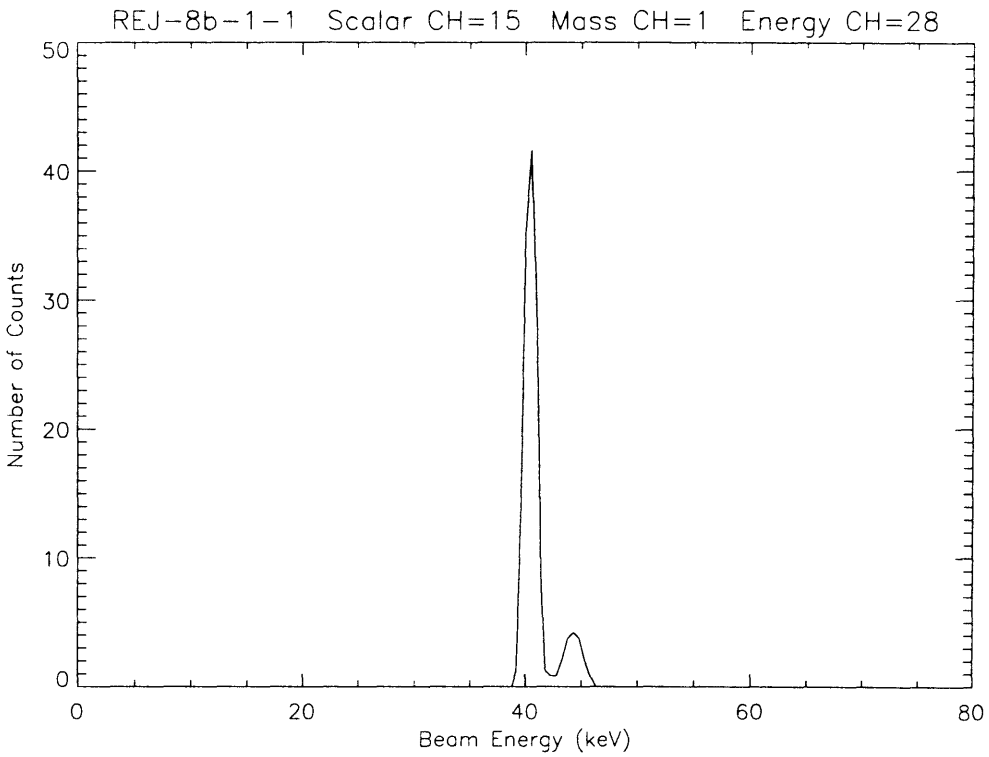

Figure 4-4: Ion Beam Energy Scan

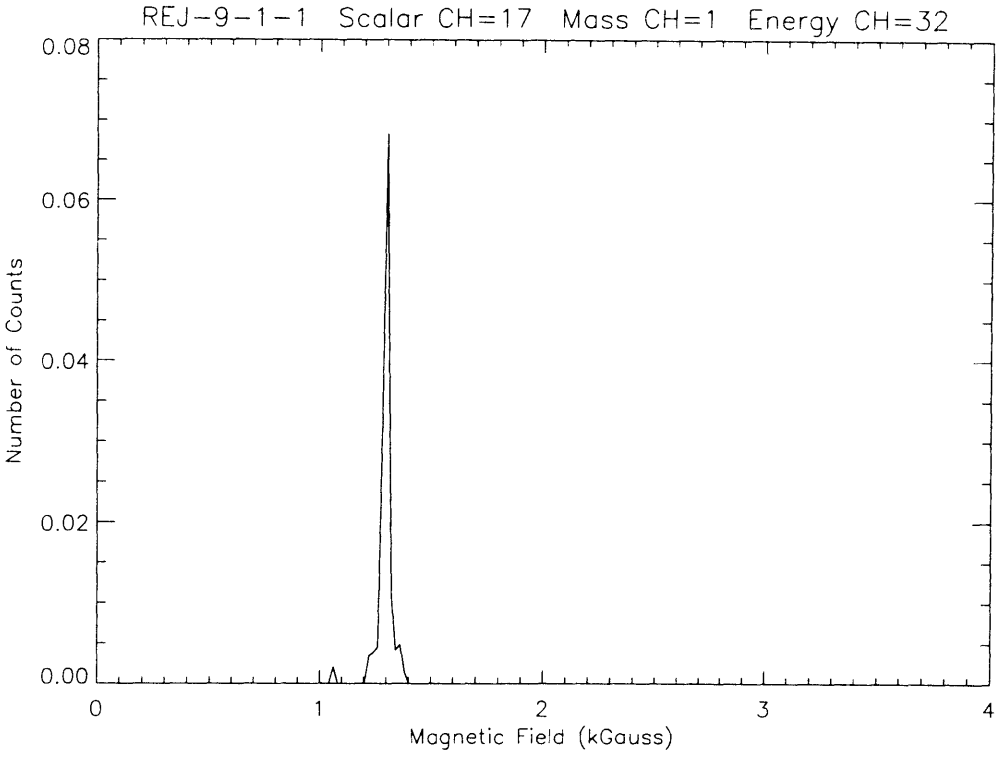

Figure 4-5: Constant Ion Beam Energy Data

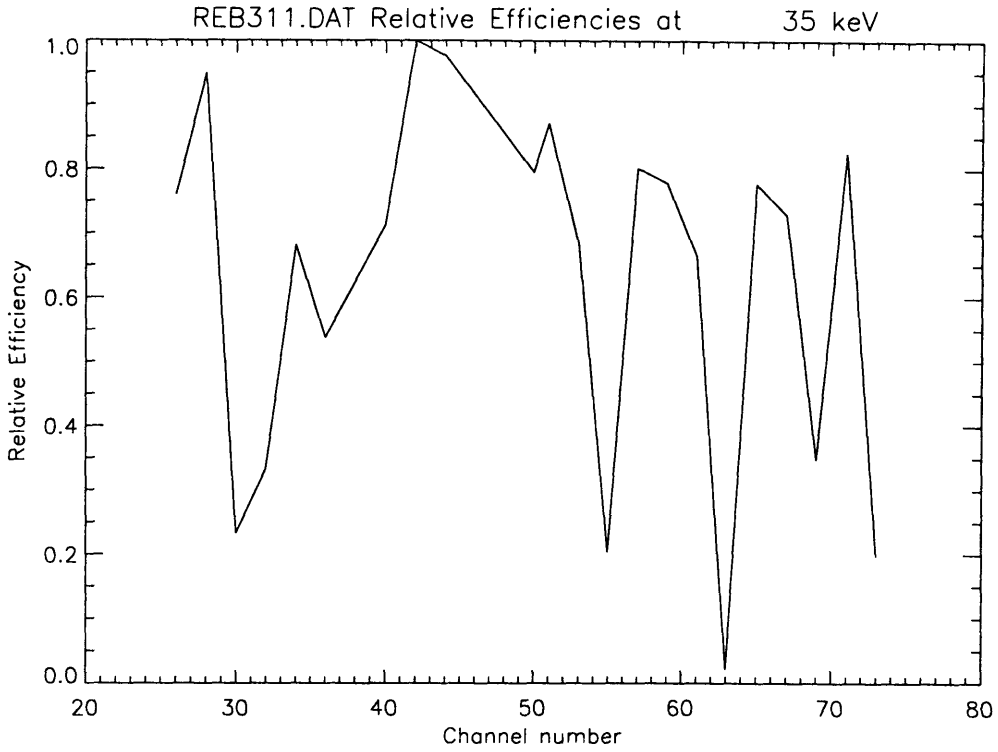

Figure 4-6: Relative Efficiencies

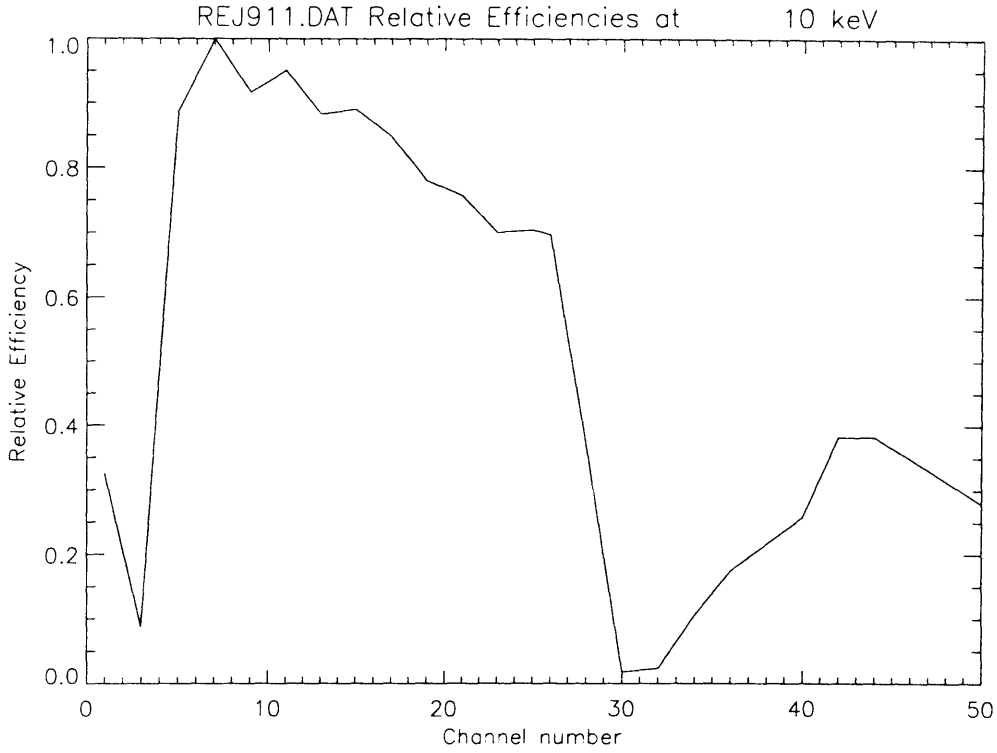

Figure 4-7: Relative Efficiencies

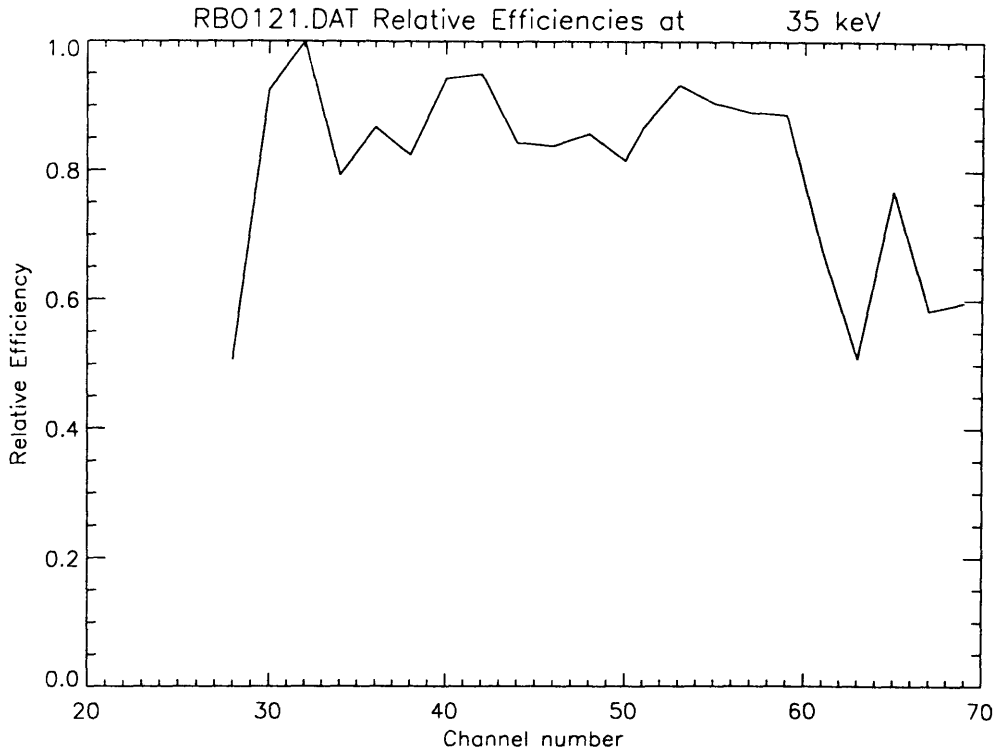

Figure 4-8: Relative Efficiencies

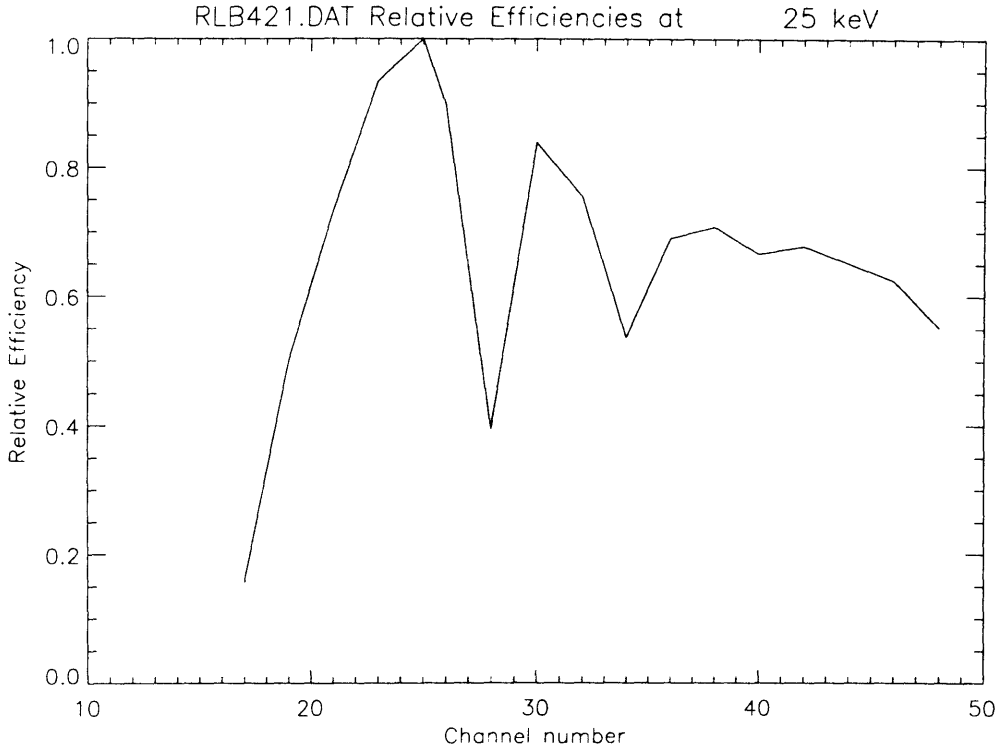

Figure 4-9: Relative Efficiencies

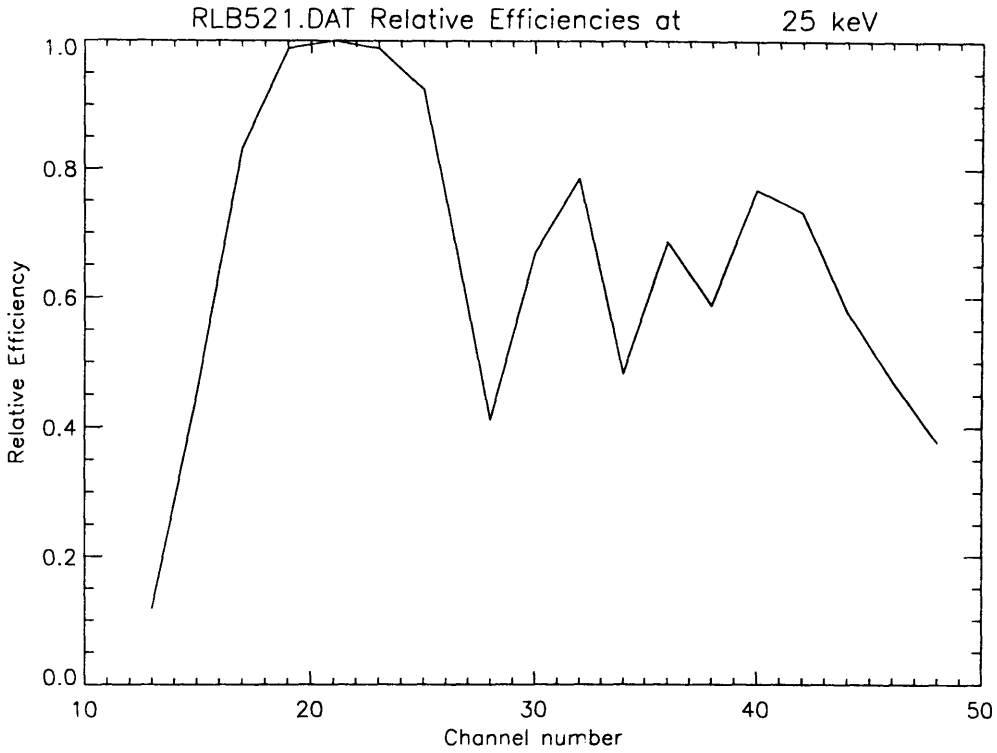

Figure 4-10: Relative Efficiencies

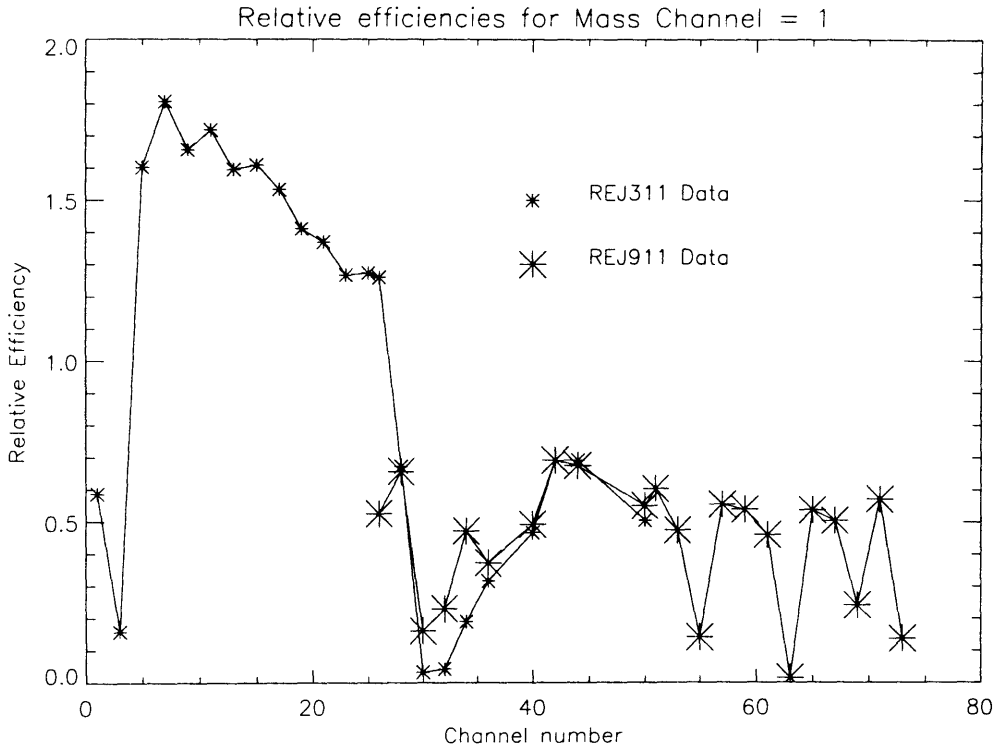

Figure 4-11: Relative Efficiencies

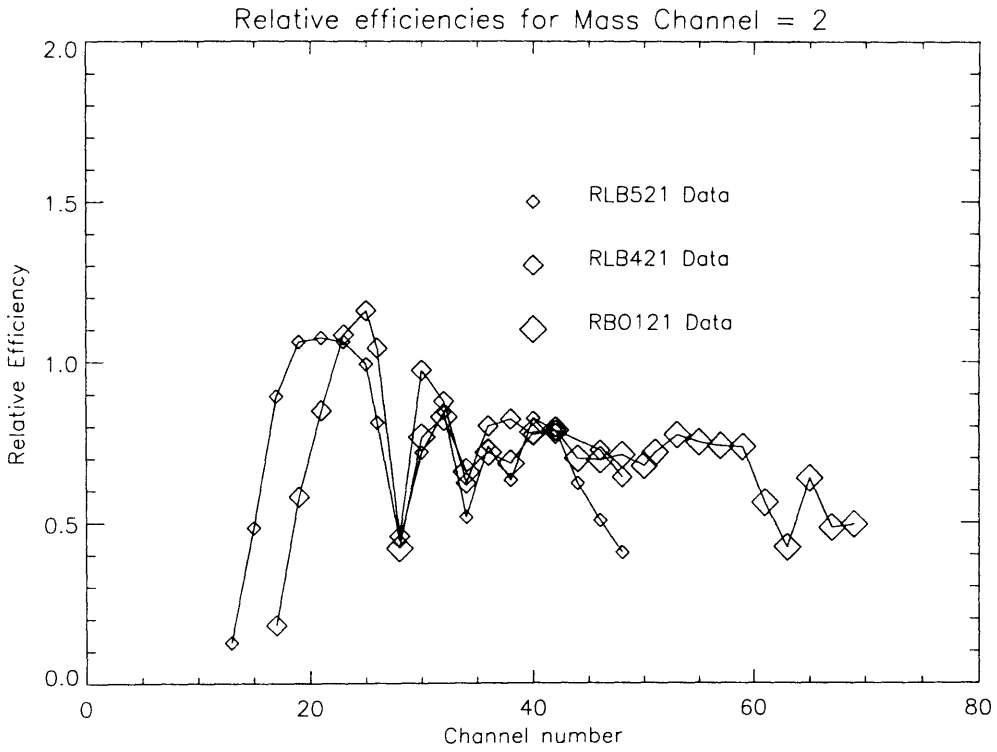

Figure 4-12: Relative Efficiencies

4.2 Cross Calibration

In the cross calibration, several reproducible plasma shots were run to provide the charge exchange neutrals for the procedure. Initially, the PCX analyzer was set up to measure ions up to a particular energy. Then the analyzer magnetic field was varied such that the energy corresponding to channel y_1 would now strike channel y_2. As will be shown, the energy range of channel y_1 does not correspond to the energy range of channel y_2. The relative efficiencies can be calculated by calculating the shift from one channel to another or by overlaying all of the data on a count rate versus energy plot and fitting a curve. The physics of the channel to channel method is shown first, then the results of the global method and the data taken from an Alcator C-Mod run are presented.

4.2.1 Channel to channel method

As shown in Equation 2.1, the magnetic field times the y-position, By, is constant. Thus, starting with a magnetic field of B_1, changing the magnetic field to B_2 will shift the position at which particles of a particular energy will strike the detectors according to:

$$\frac{y_1}{y_2} = \frac{B_2}{B_1} \tag{4.1}$$

Then, knowing Equation 2.1, we can also derive the dependence of ΔK upon B and y.

$$B(Tesla) = 0.915 \frac{\sqrt{Km}}{qy_f}$$

$$K = Const^2 B^2 y^2$$

So for the energy range, ΔK, of a channel of half width Δy, compute the upper and lower bounds, ΔK^L and ΔK^U.

$$\Delta K_1^L = Const^2 B_1^2 [y_1^2 - (y_1 - \Delta y)^2]$$

and

$$\Delta K_2^L = Const^2 B_2^2 [y_2^2 - (y_2 - \Delta y)^2]$$

Then

$$\frac{\Delta K_2^L}{\Delta K_1^L} = \frac{Const^2 B_2^2 [y_2^2 - (y_2^2 - 2y_2 \Delta y + \Delta y^2)]}{Const^2 B_1^2 [y_1^2 - (y_1^2 - 2y_1 \Delta y + \Delta y^2)]}$$

Which reduces to:

$$\frac{\Delta K_2^L}{\Delta K_1^L} = \frac{B_2^2 y_2^2}{B_1^2 y_1^2} \frac{\Delta y^2 / y_2 - 2\Delta y}{\Delta y^2 / y_1 - 2\Delta y}$$

Since $(\frac{\Delta y}{y_x})^2 \approx (\frac{0.2}{10})^2 = 0.0004$, it can be taken as 0. So then,

$$\frac{\Delta K_2^L}{\Delta K_1^L} = \frac{B_2^2}{B_1^2} (\frac{y_2}{y_1})^2 \frac{-2\Delta y / y_2}{-2\Delta y / y_1} = \frac{B_2^2}{B_1^2} (\frac{y_2}{y_1})^2 \frac{y_1}{y_2} = \frac{B_2^2}{B_1^2} \frac{y_2}{y_1}$$

But, recall Equation 4.1, and $\frac{y_2}{y_1} = \frac{B_1}{B_2}$, so

$$\frac{\Delta K_2^L}{\Delta K_1^L} = \frac{B_2^2}{B_1^2} \frac{B_1}{B_2} = \frac{B_2}{B_1} = \frac{y_1}{y_2} \tag{4.2}$$

Similarly for ΔK_1^U and ΔK_2^U,

$$\Delta K_1^U = C^2 B_1^2[(y_1 + \Delta y)^2 - y_1^2]$$

and

$$\Delta K_2^U = C^2 B_2^2[(y_2 + \Delta y)^2 - y_2^2]$$

Then

$$\frac{\Delta K_2^U}{\Delta K_1^U} = \frac{C^2 B_2^2[(y_2 + \Delta y)^2 - y_2^2]}{C^2 B_1^2[(y_1 + \Delta y)^2 - y_1^2]}$$

$$\frac{\Delta K_2^U}{\Delta K_1^U} = \frac{B_2^2}{B_1^2}(\frac{y_2}{y_1})^2 \frac{\Delta y^2/y_2^2 + 2\Delta y/y_2}{\Delta y^2/y_1^2 + 2\Delta y/y_1}$$

Again, $(\frac{\Delta y}{y_x})^2 \approx 0$,

$$\frac{\Delta K_2^U}{\Delta K_1^U} = \frac{B_2^2}{B_1^2}(\frac{y_2}{y_1})^2 \frac{2\Delta y/y_2}{2\Delta y/y_1} = \frac{B_2^2}{B_1^2}(\frac{y_2}{y_1})^2 \frac{y_1}{y_2} = \frac{B_2^2}{B_1^2}\frac{y_2}{y_1}$$

Recall also that $\frac{y_2}{y_1} = \frac{B_1}{B_2}$,

$$\frac{\Delta K_2^U}{\Delta K_1^U} = \frac{B_2^2}{B_1^2}\frac{B_1}{B_2} = \frac{B_2}{B_1} = \frac{y_1}{y_2} \tag{4.3}$$

Since ΔK is just $\Delta K^U + \Delta K^L$, then using Equations 4.2 and 4.3,

$$\Delta K_2 = \Delta K_2^U + \Delta K_2^L = \Delta K_1^U \frac{y_1}{y_2} + \Delta K_1^L \frac{y_1}{y_2} = \Delta K_1 \frac{y_1}{y_2}$$

So then we see that

$$\frac{\Delta K_2}{\Delta K_1} = \frac{y_1}{y_2} \tag{4.4}$$

To a first order then, the counting rate in the new channel, at y_2, would be $\approx \frac{y_1}{y_2}$ times the counting rate in the first channel, at y_1.

However, the flux, and hence the counting rate, is a function of energy. To see the order of the error which neglecting this dependence would cause, let's consider a simple plasma with a Maxwellian ion velocity distribution such that the ion temperature is 1.5 keV. If the first channel is channel 2 ($y_2 = 14.50$ cm), is measuring 2 keV particles, then from Equation 2.1, the energy range it views can be used to determine the number of counts that it will detect.

$$B = 0.915\frac{\sqrt{Km}}{qy} \qquad \rightarrow \frac{y}{\sqrt{K}} = constant$$

$$K_2^L = \frac{(2\ keV)(14.25)^2}{14.50^2} = 1.93\ keV$$

$$K_2^U = \frac{(2\ keV)(14.75)^2}{14.50^2} = 2.07\ keV$$

If we move this to channel 4 ($y_4 = 16.50$ cm), then the simple approach would predict the ratio of counts to be $\frac{14.50}{16.50} = 0.8788$. To use the more accurate method, compute the upper and lower energies detected by channel 4:

$$K_4^L = \frac{(2\ keV)(16.25)^2}{16.50^2} = 1.94\ keV$$

$$K_2^U = \frac{(2\ keV)(16.75)^2}{16.50^2} = 2.06\ keV$$

We know that $\frac{d}{dK}[\ln(\frac{dN}{dK})]$ is -1.5, if we ignore the energy dependence of $< \sigma_{cx}\, v >$. If we set $\ln(\frac{dN}{dK}) = 8$ at 2 keV, then we can compute the counts in each channel.

$$\frac{dN}{dK} = \exp(-1.5(K - \frac{22}{3})) \quad \rightarrow N = \exp[\frac{-3}{2} - \frac{22}{3}]\frac{[\exp(-1.5K)]_{K_L}^{K_U}}{-1.5}$$

$$N_2 = \frac{\exp(11)}{-1.5}[\exp((-1.5)(2.0696) - \exp((-1.5)(1.9316))] = 411.74$$

$$N_4 = \frac{\exp(11)}{-1.5}[\exp((-1.5)(2.0611) - \exp((-1.5)(1.9399))] = 361.52$$

$$\frac{N_4}{N_2} = 0.87803 \approx 0.8788$$

So the energy differences are small enough that the simple approach will work.

In theory, this method should suffice to determine the relative calibration of the MCP channels. However, the calculations are rather tedious and have acknowledged (though small) errors which could cause problems. Instead, an easier and more efficient way has been used to analyze the data from the calibration runs on Alcator C-Mod.

4.2.2 Global fit method

The second method of cross channel calibration is to overlay the results from several repeated plasma shots and to fit the results to a curve. Since the energy dependence of the electric and magnetic fields is well established, a plot of neutral particle flux versus energy can be established. The same plasma shots could be used for both this method and the first method of cross calibration.

The results of 8 Alcator C-Mod plasma shots, which were run on January 10th, 1995 (shots 950110xxx), were overlaid and empirically fit to a high order polynomial (4th order) using an IDL program. The central electron density for these shots was around $1.1 \times 10^{14} cm^{-3}$, the central electron temperature was around 2 keV, and the plasma temperature was around 1.3keV. The plasma current was 800 kAmp, with a toroidal magnetic field of 5.3 Tesla. Figure 4-13 shows the data from the mass 2 row. The equation from the fitting is that the flux of a channel is related to the energy of that channel, K, by:

$$flux = 36.9095 - 3.8780K_p + 0.4850K_p^2 - 3.8271 \times 10^{-2}K_p^3 + 1.2064 \times 10^{-3}K_p^4$$

A least squares polynomial fit was used to determine the average flux at each energy. For each channel, the average of the ratio of the data to the fit was taken to be the relative efficiency of that MCP channel if and only if the variation is systematic, and not shot related. The resulting relative efficiencies for all 8 shots for channels 1-7 are shown in Figure 4-14, channels 8-14 are in Figure 4-15, channels 15-21 in Figure 4-16, 22-29 in Figure 4-17, and 30-39 in Figure 4-18. Note that channel 33 was not operating for these shots, and so channels 34-39 show up as channels 33-38. The relative efficiencies for all the channels is shown in Figure 4-19. Channel 1 is shown on all of the plots for comparison.

From these results, it is apparent that channels 1-8 have large variations in the calculated relative efficiencies. This is due to the large variations in the counting rates at energies close to to the plasma temperature, so the variation is more attributable to the plasma conditions than to the relative efficiencies. Channels 8-38 have a more systematic deviation from the normalization of the fluxes, which is attributable to the relative efficiencies. The counting rate in channel 39 was too low for proper statistics, hence the large variation in its relative efficiency.

The final results of the relative efficiency calculations for mass row 2 are shown in Table 4.1. Mass row 1 was analyzed in a similar fashion, with similar results. The relative efficiencies for mass row 1 are plotted in Figure 4-20.

Table 4.1: MCP Mass Row 2 Relative Efficiencies

Channel	Relative efficiency
1	0.802
2	0.413
3	1.708
4	1.115
5	1.183
6	1.755
7	1.080
8	1.059
9	0.952
10	0.948
11	0.883
12	0.884
13	0.902
14	0.795
15	1.294
16	1.021
17	1.409
18	1.120
19	0.972
20	1.032
21	0.979
22	0.953
23	0.913
24	1.058
25	1.107
26	1.033
27	0.949
28	0.869
29	0.923
30	0.869
31	0.894
32	0.834
33	N/A
34	0.984
35	0.784
36	1.005
37	0.615
38	0.787
39	1.950

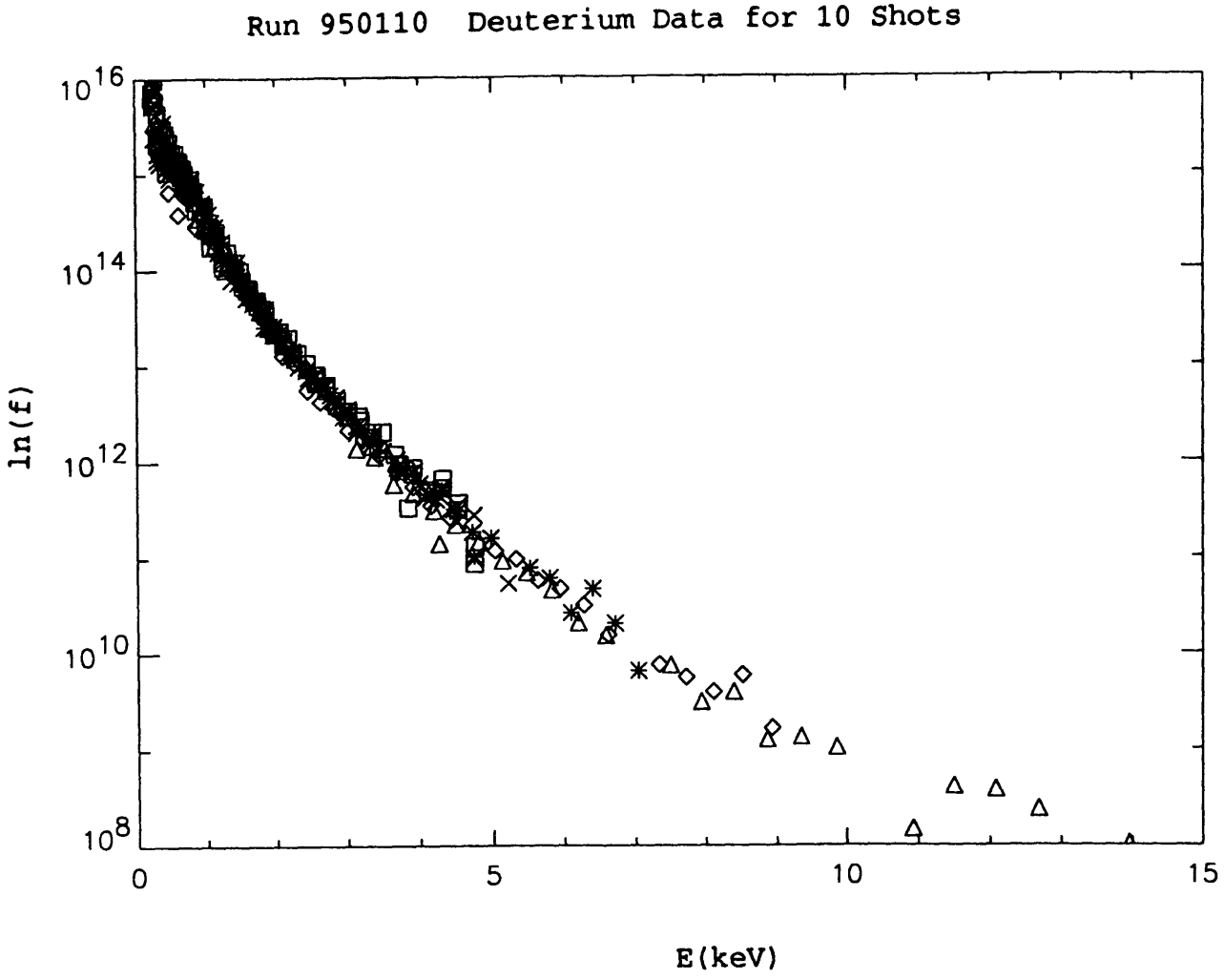

Figure 4-13: Mass Row 2 Neutral particle Flux vs. Energy

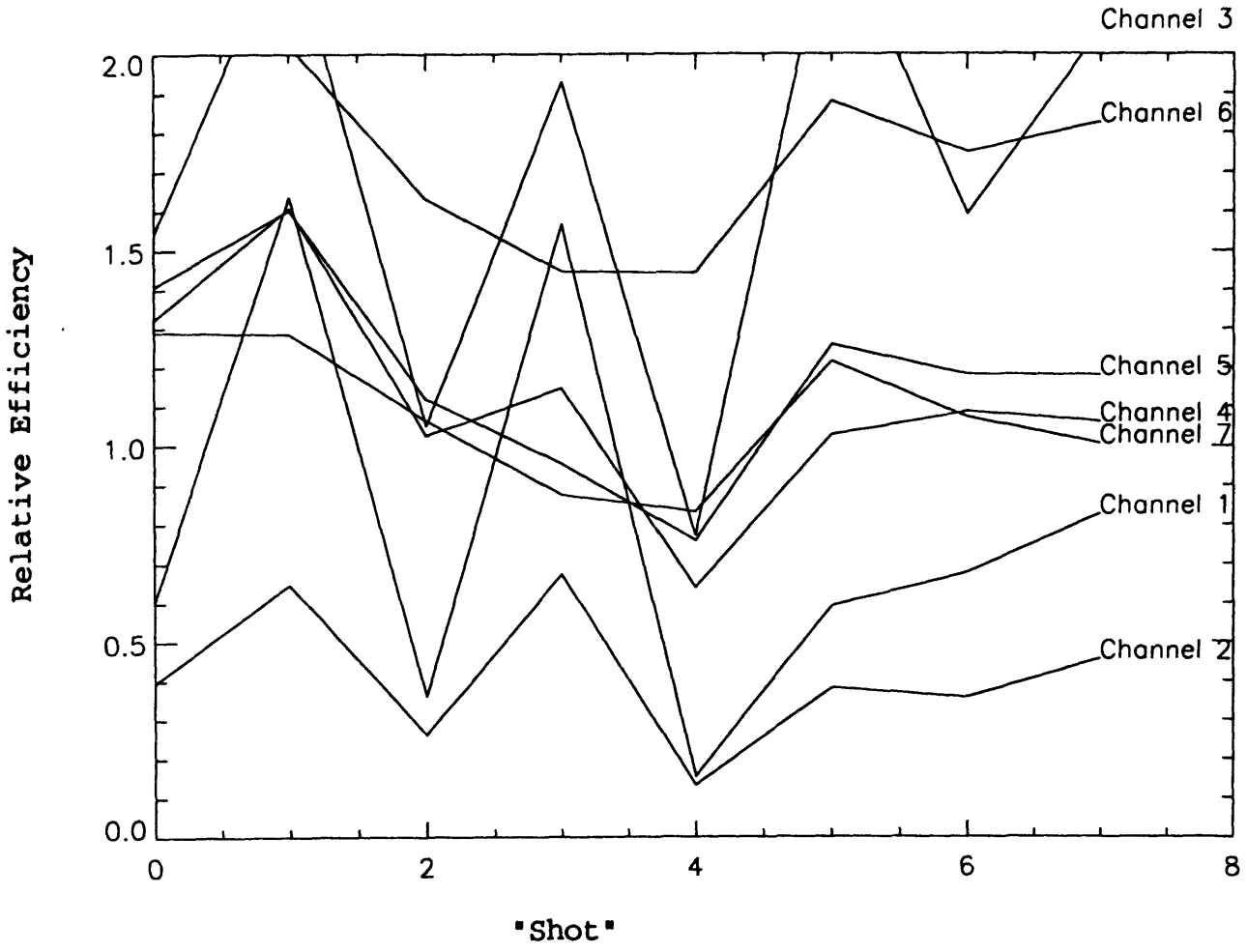

Figure 4-14: All 8 shots, Mass Row 2 channels 1-7

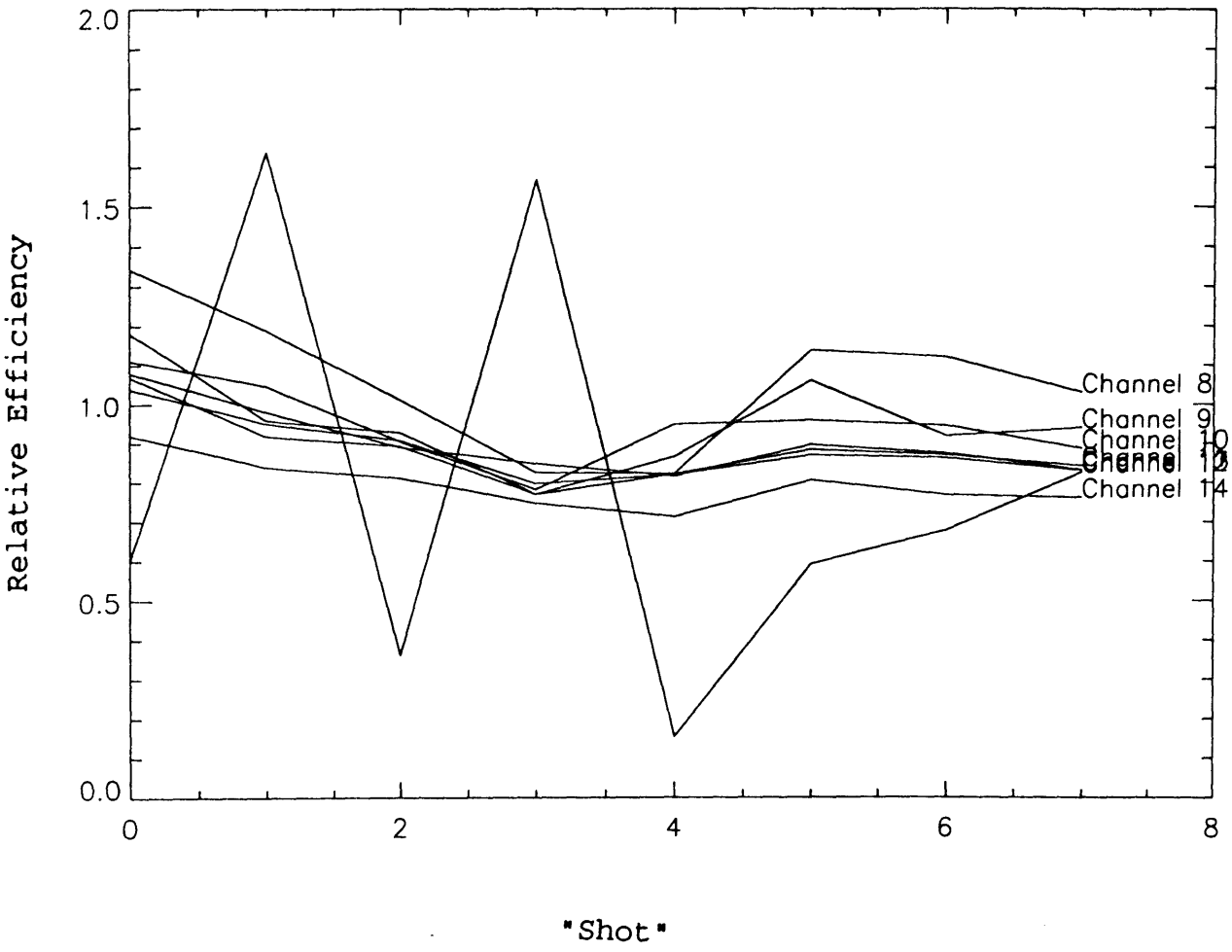

Figure 4-15: All 8 shots, Mass Row 2 channels 8-14

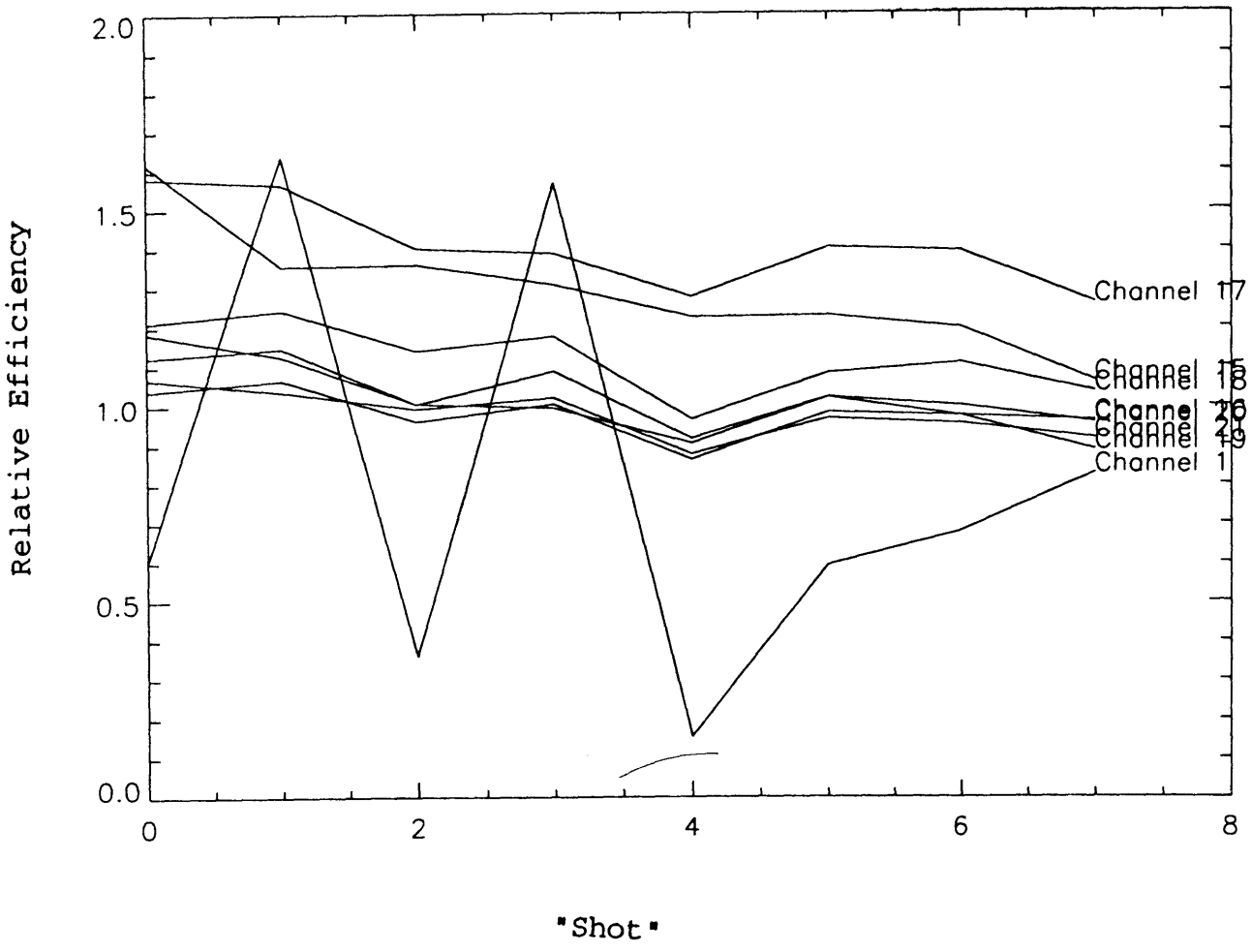

Figure 4-16: All 8 shots, Mass Row 2 channels 15-21

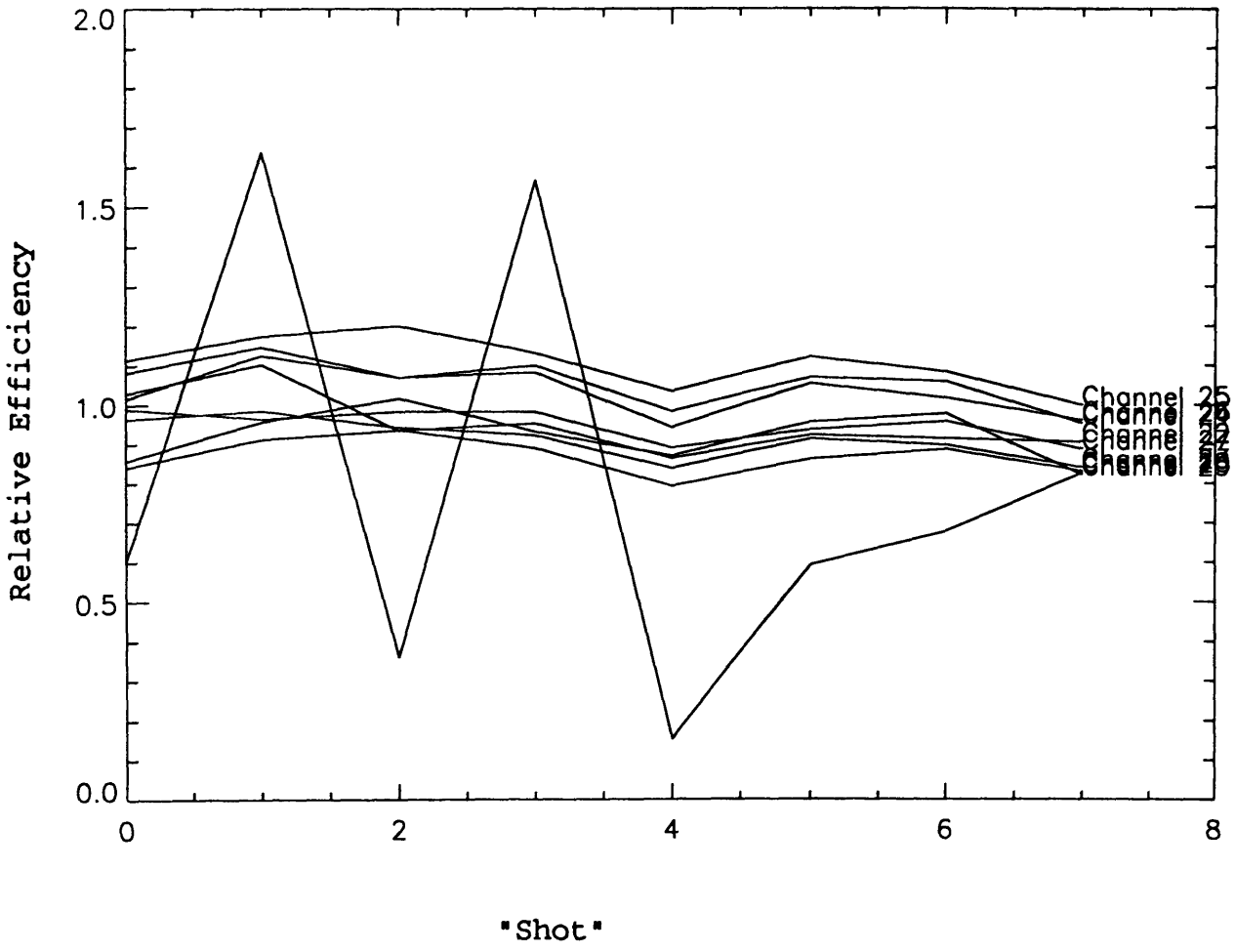

Figure 4-17: All 8 shots, Mass Row 2 channels 22-29

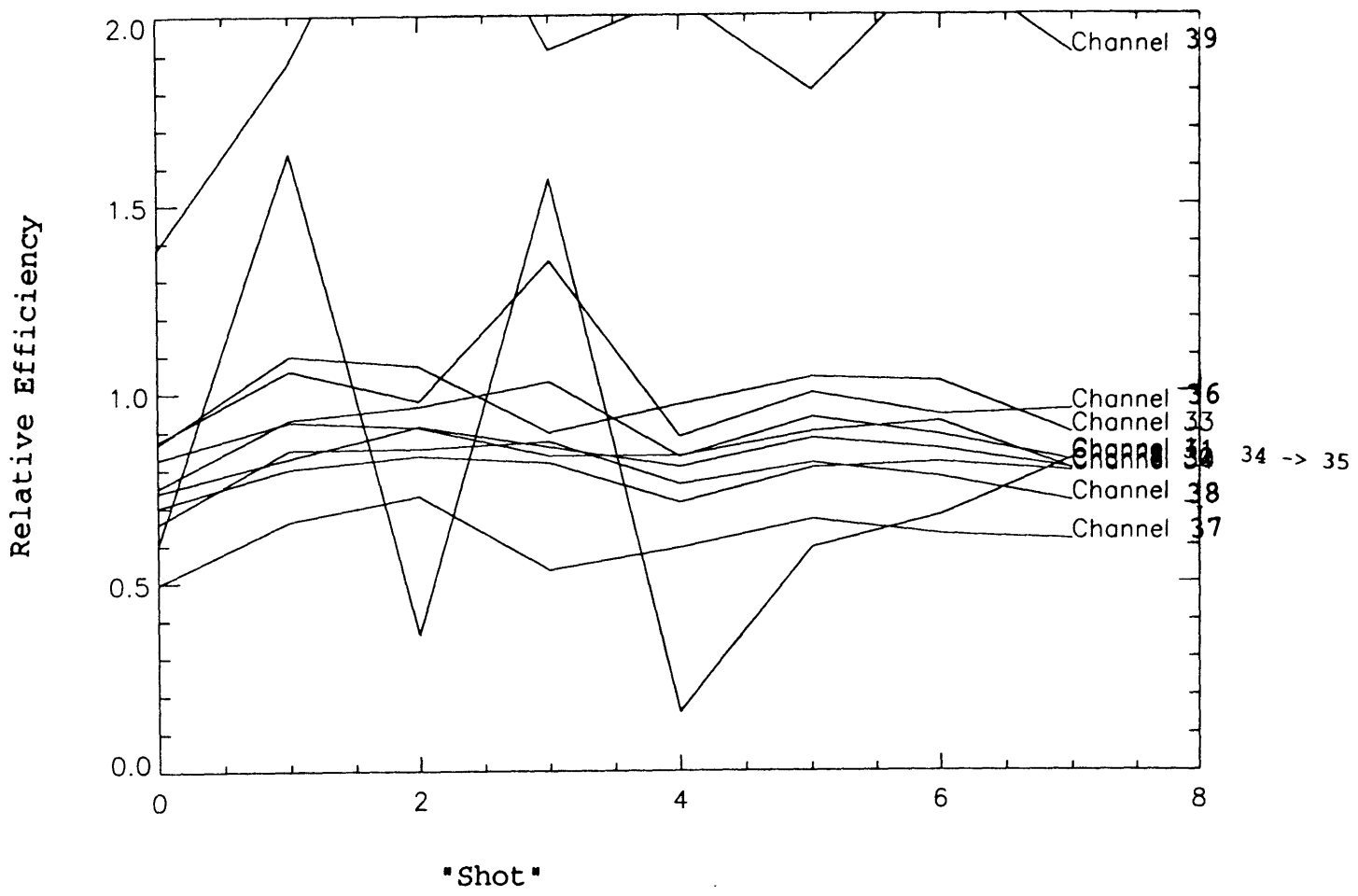

Figure 4-18: All 8 shots, Mass Row 2 channels 30-39

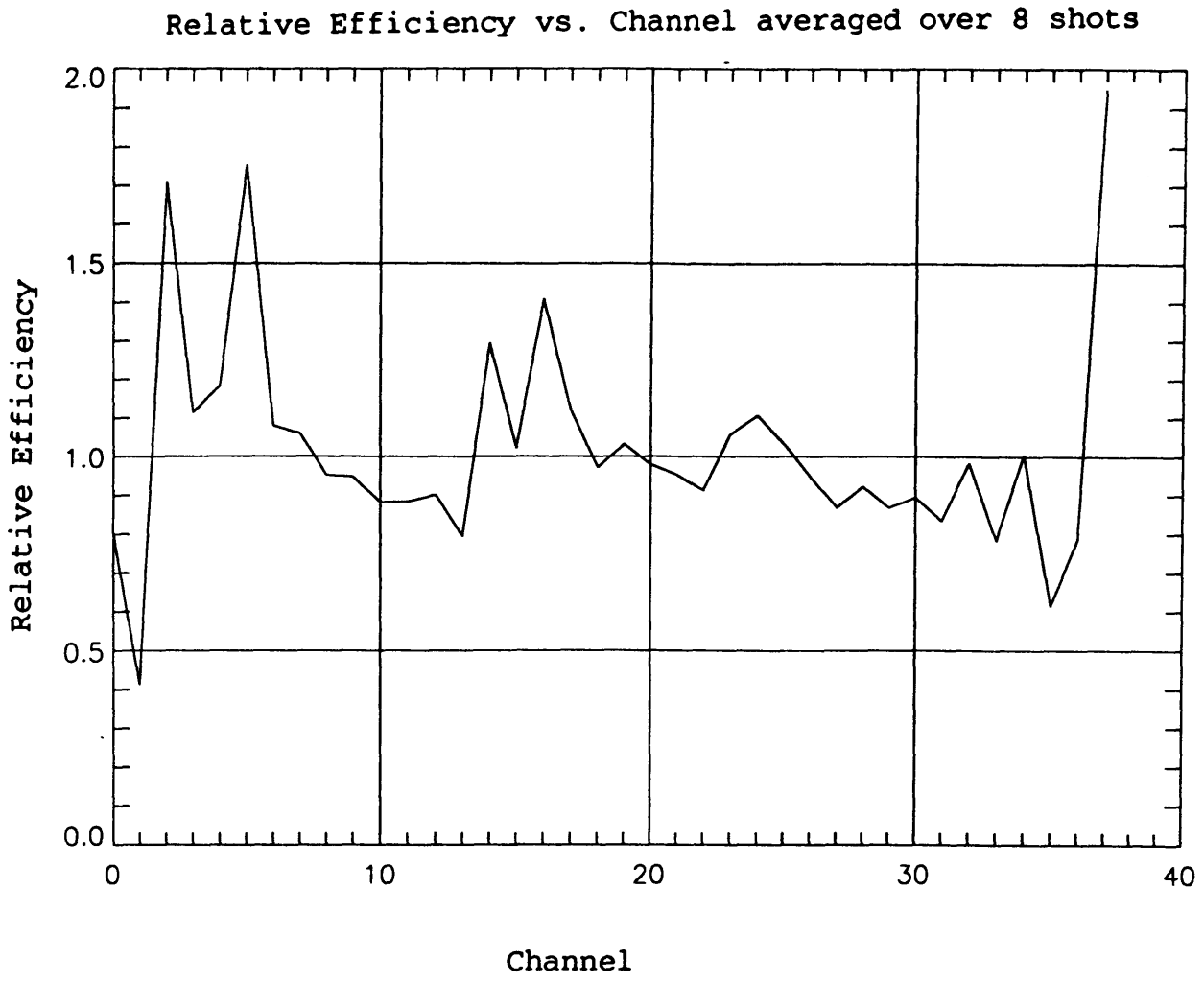

Figure 4-19: All 8 shots, all Mass Row 2 channels

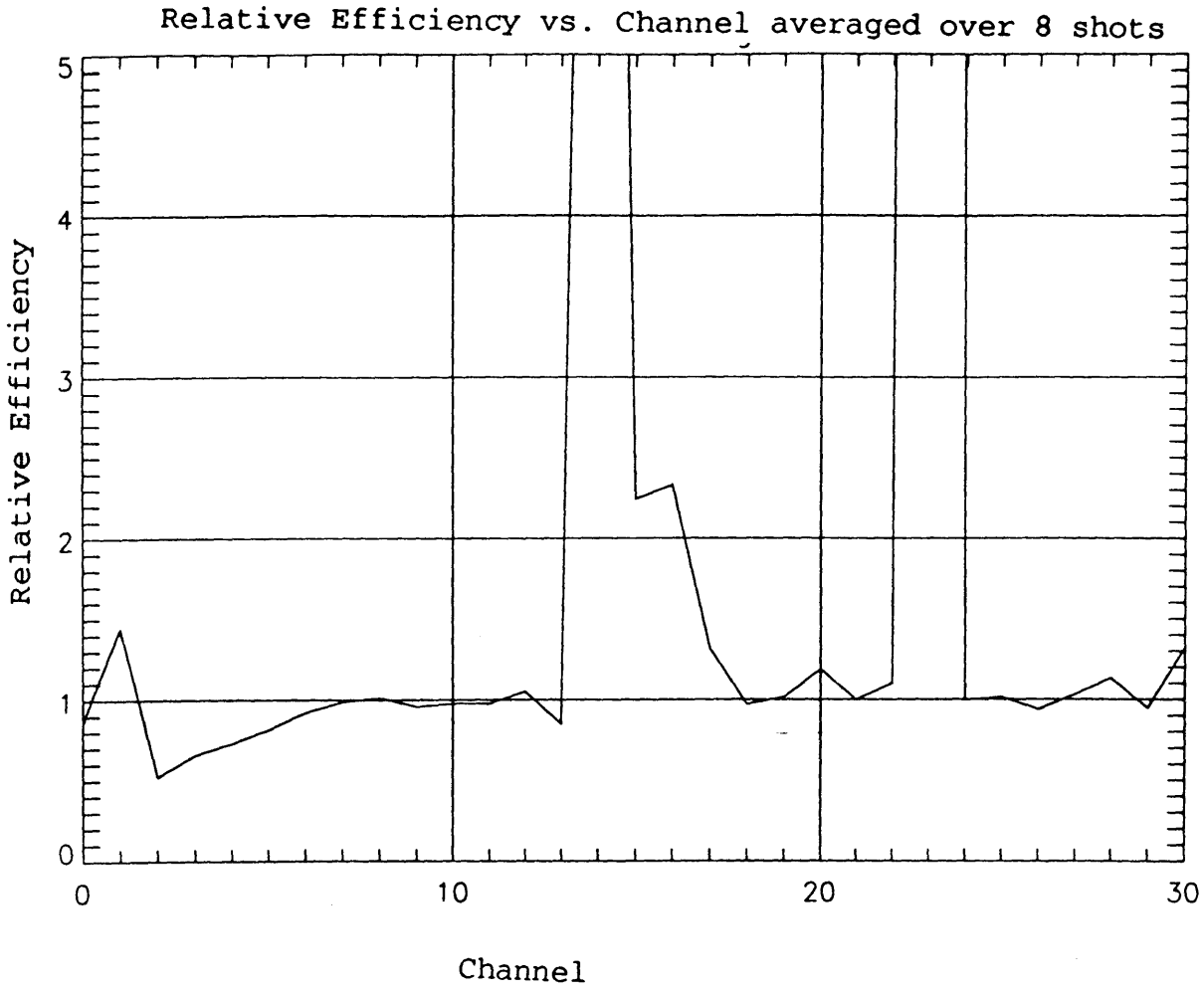

Figure 4-20: All 8 shots, all Mass Row 1 channels

Chapter 5

Parametric Study

To determine the range of plasma parameters for which the PCX analyzer should give reasonable data, a Fokker-Planck simulation code was utilized. FPPRF [9], programmed by Greg Hammet, was used to determine the effects of varying the electron and ion temperatures and densities.

FPPRF is a Fokker-Planck code with a bounce averaged quasilinear operator which takes into account ICRF local resonance heating. FPPRF can show the charge exchange neutral flux that leaves the plasma. To produce the neutral particle flux, the dependence upon the ion temperature and density, the neutral atom densities in the plasma, and the various collisional mechanisms are taken into account. FPPRF also takes into account the line of sight of the analyzer, and hence the pitch angle dependence of RF generated fast ions.

For this analysis, FPPRF was run with a 403 point energy grid. A 1% hydrogen minority concentration and a 4.5% carbon impurity concentration were used. The Fokker-Planck equation was solved for the deuterium majority. As mentioned in Chapter 2, the neutral density used by FPPRF gave an edge neutral density of

10^{12} cm^{-3}. The charge exchange neutral particle flux was analyzer 1 millisecond into the run, which is sufficient due to the steady state nature of this analysis. The plasma was taken to have its magnetic axis located at a major radius of 68.0 cm. A loop voltage of 1.0 volts was used with a toroidal magnetic field strength of 5.3 Tesla and a plasma current of 710 kAmp to simulate typical Alcator C-Mod Ohmic plasma parameters.

The analysis of the data assumed the PCX analyzer would be configured to look at particles with up to 50 keV energy. A fit of the stripping cell efficiency was used in conjunction with the actual analyzer parameters (calculated in chapter 3) to determine the counting rates. The polynomial fit of the stripping cell efficiency is shown in Equation 5.1 where k_{en} is the particle energy in keV divided by the mass in amu.

$$\varepsilon_s = -0.2+0.072k_{en}-0.61\times10^{-2}k_{en}^2+0.24\times10^{-3}k_{en}^3-0.45\times10^{-5}k_{en}^4+0.32\times10^{-7}k_{en}^5 \tag{5.1}$$

The fast neutral particle flux is used to compare the ion temperature which a charge exchange analyzer would detect to the ion temperature which FPP has used. The particle flux from FPPRF was also used to determine the counting rates which the analyzer detectors would show by taking into account the stripping cell efficiency, the actual detector locations, the solid angle and field of view, and the analyzer's magnetic and electric field strengths. An example of the results of this analysis is shown in Figure 5-1.

The predicted analyzer counting rates were then used to determine what range of energies of the FPP neutral particle flux would be appropriate to use for calculating the temperature which the charge exchange analyzer would measure. For

proper statistics, a counting rate of more than 1 particle per millisecond per channel is needed in the detector channels. This is also to help overcome noise and counts from other types of radiation, such as neutrons and high energy X-rays. Then the FPP flux was analyzed for the energy range which would meet these criteria.

The slope of the natural log of the FPP flux plotted against particle energy gives the negative inverse of the ion temperature, as in Equation 2.7. This calculated temperature is then compared to the actual temperature which FPPRF used to determine how appropriate the charge exchange analyzer ion temperature would be. The temperature is simply: $-\frac{1}{T_i} = \frac{d}{dK} \ln(\Gamma_{FPP})$.

The temperature was varied by changing the ion temperature on axis and scaling the edge temperature, the electron temperature on axis, and the electron edge temperature accordingly. The electron density on axis was also varied, and the edge electron density was scaled with the central density.

Figures 5-2 to 5-26 show the FPPRF neutral flux, the line fitted to the flux for the appropriate energy range (as previously mentioned), and the temperature the analyzer would measure. For the plots that do not have the fitted line, and hence a temperature from the fit, there were not enough channels with acceptable counting rates from which to calculate a temperature. Figure 5-27 shows the computed temperature compared to the FPPRF temperature at an electron densities of 0.5, 1.0, 2.0, and $3.0 \times 10^{14}\ m^{-3}$.

From Figure 5-27, it is clear that temperature measured via charge exchange analysis will consistently underpredict the actual temperature for an Ohmic plasma, though the results both below $n_e \approx 10^{14}\ cm^{-3}$ and $T_i \approx 1$ keV were not excessively inaccurate. This is due in part to better transmission, both from lower ionization cross sections at the lower temperatures and from the lower density of ionizing

particles.

This study did not explore the effects of different profile shapes, auxiliary heating, enhanced confinement modes (such as H-mode), or off axis sightlines, all of which may affect the charge exchange data. However, knowing the difficulties involved in measuring the temperature from the charge exchange neutral particle flux is an important result. Future work could explore the other parameters mentioned.

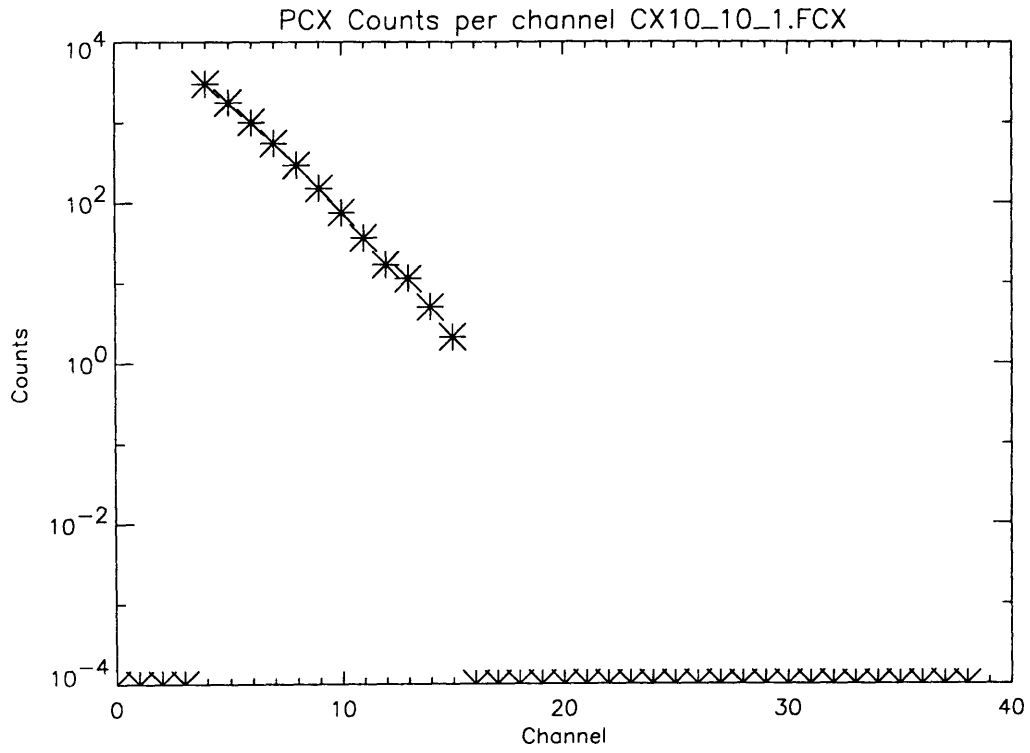

Figure 5-1: Predicted PCX Count Rate

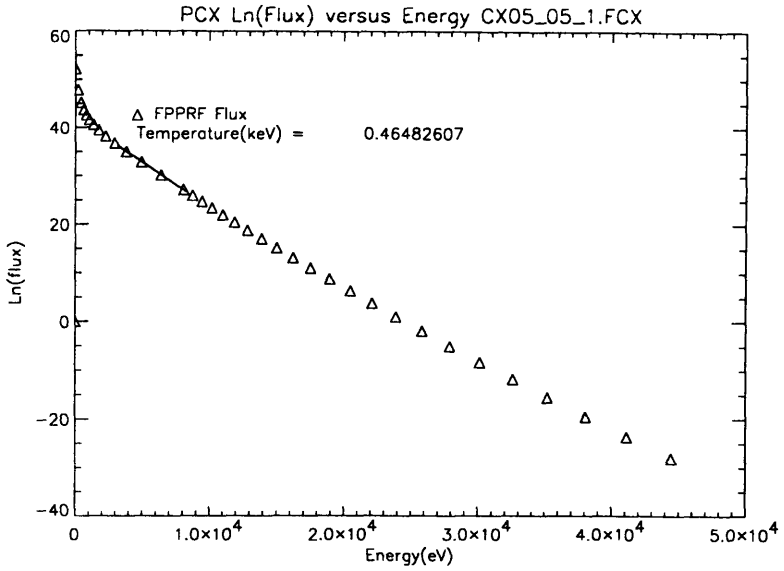

Figure 5-2: FPP Flux versus Energy with Fit

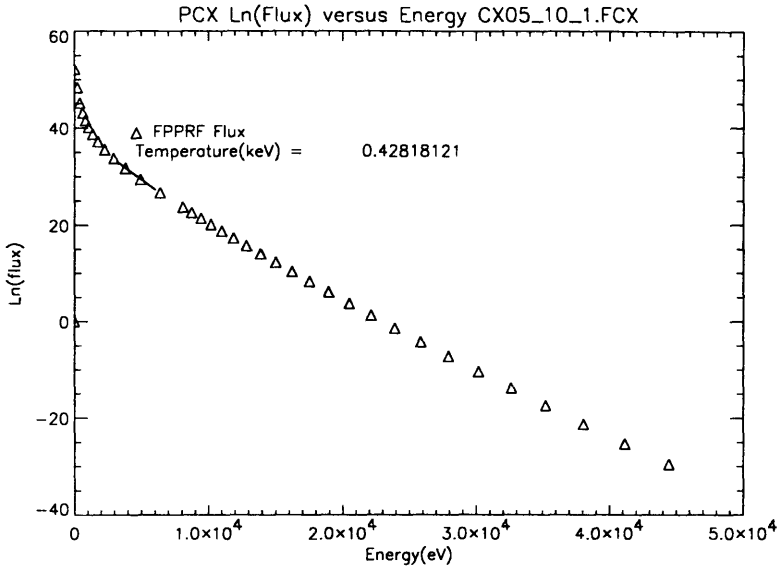

Figure 5-3: FPP Flux versus Energy with Fit

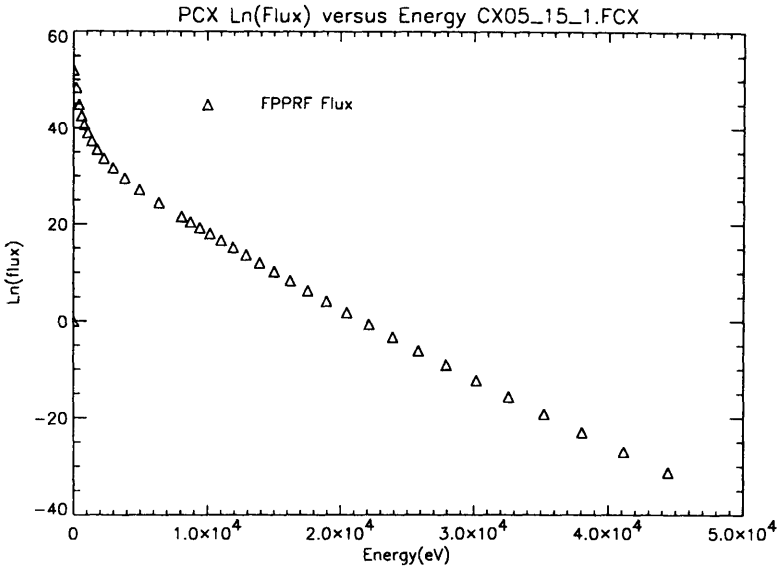

Figure 5-4: FPP Flux versus Energy with Fit

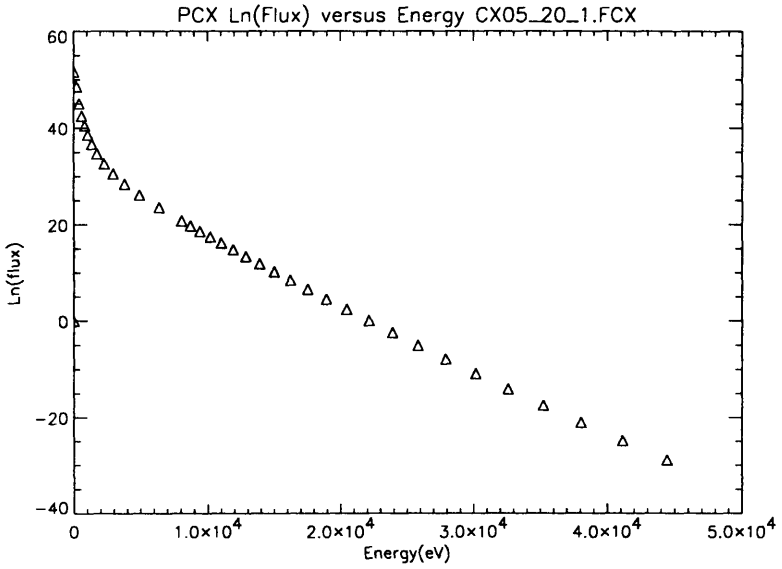

Figure 5-5: FPP Flux versus Energy with Fit

PAGES (S) MISSING FROM ORIGINAL

PAGE 89 MISSING

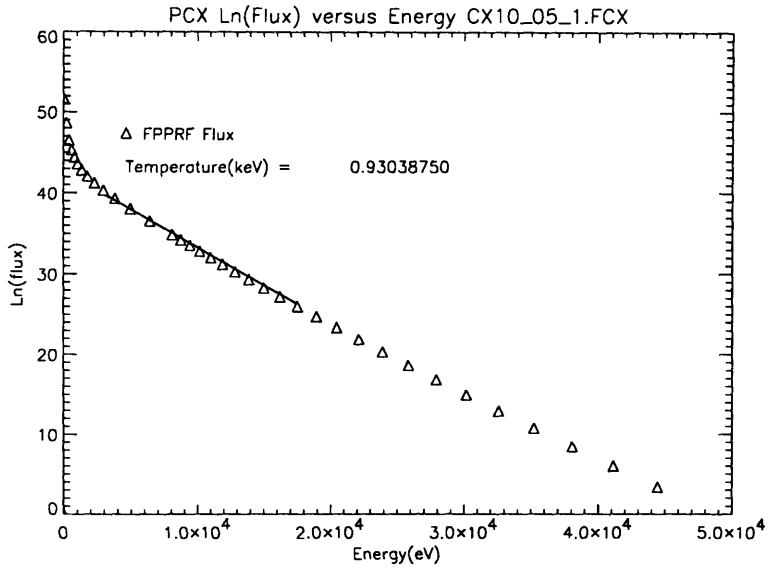

Figure 5-7: FPP Flux versus Energy with Fit

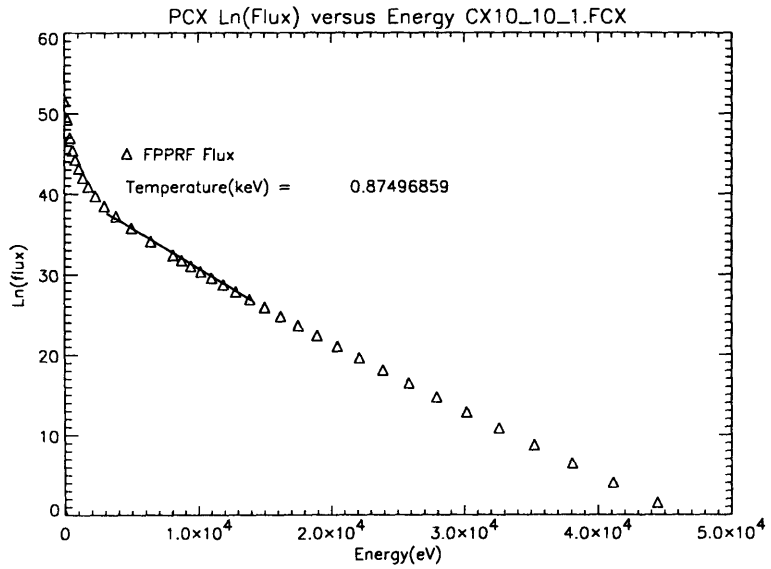

Figure 5-8: FPP Flux versus Energy with Fit

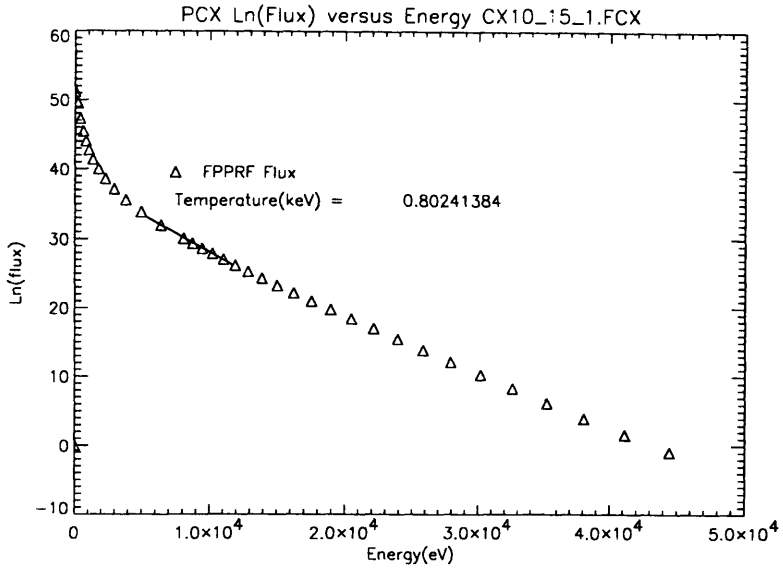

Figure 5-9: FPP Flux versus Energy with Fit

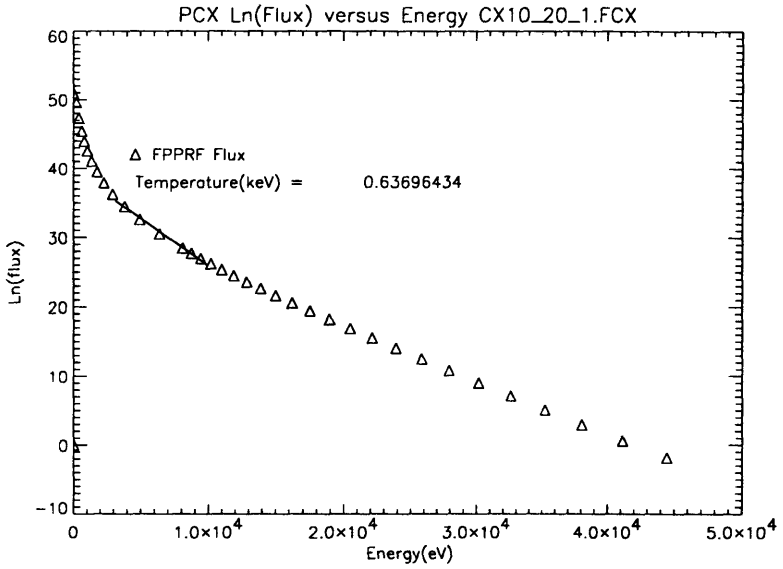

Figure 5-10: FPP Flux versus Energy with Fit

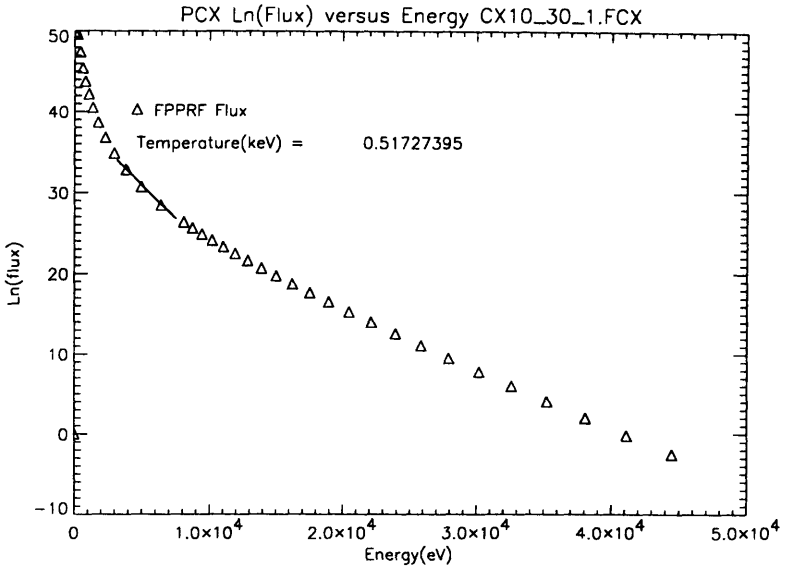

Figure 5-11: FPP Flux versus Energy with Fit

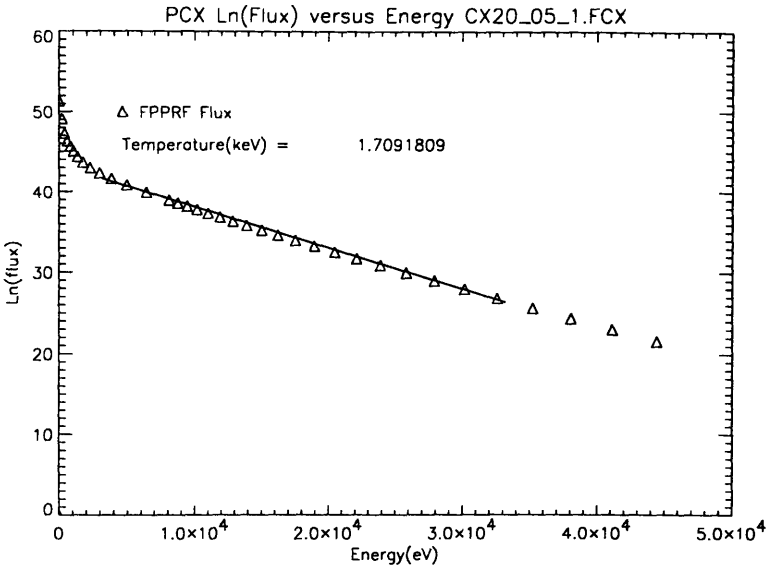

Figure 5-12: FPP Flux versus Energy with Fit

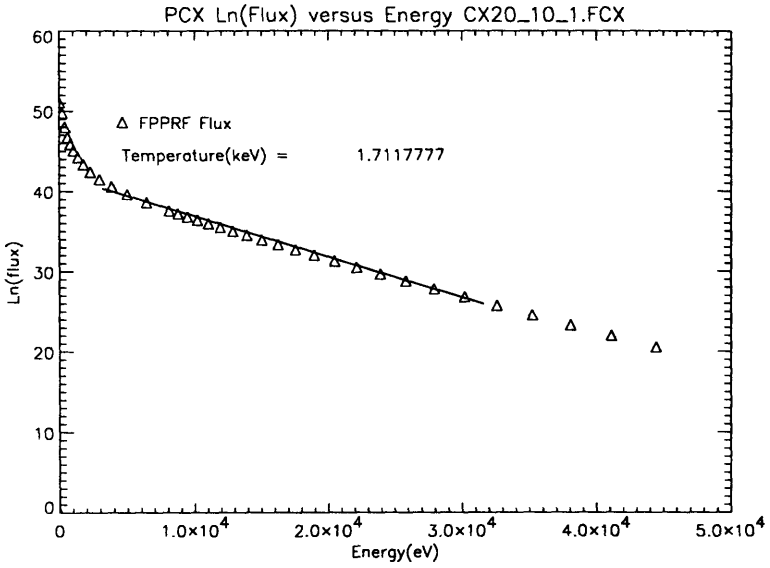

Figure 5-13: FPP Flux versus Energy with Fit

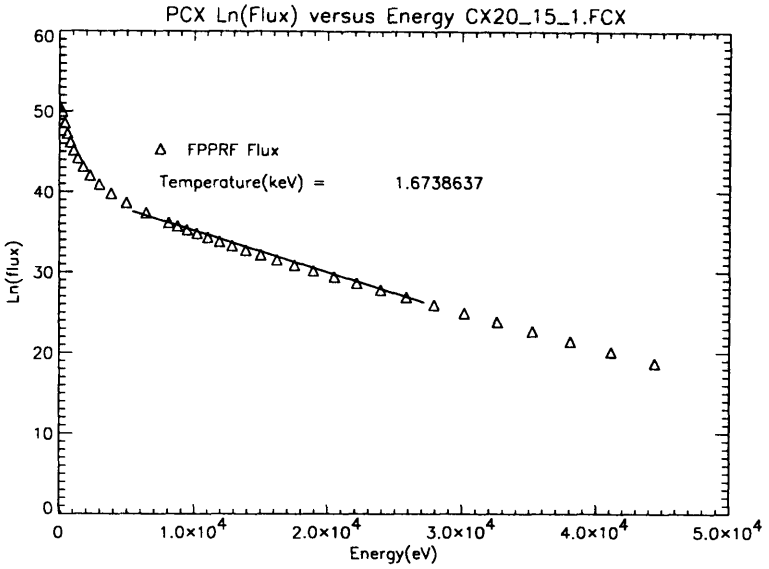

Figure 5-14: FPP Flux versus Energy with Fit

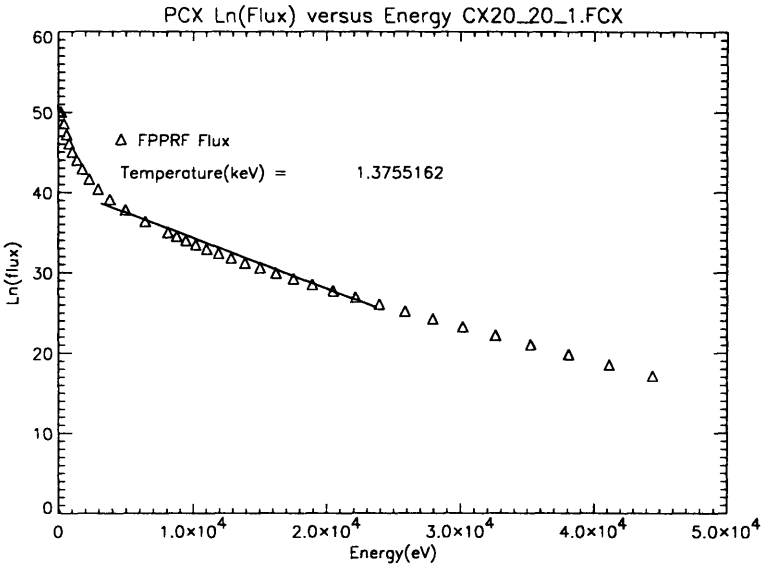

Figure 5-15: FPP Flux versus Energy with Fit

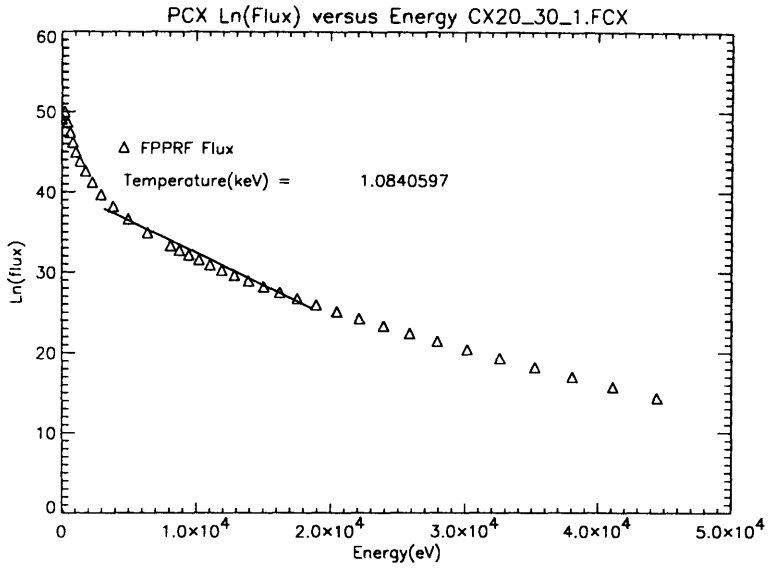

Figure 5-16: FPP Flux versus Energy with Fit

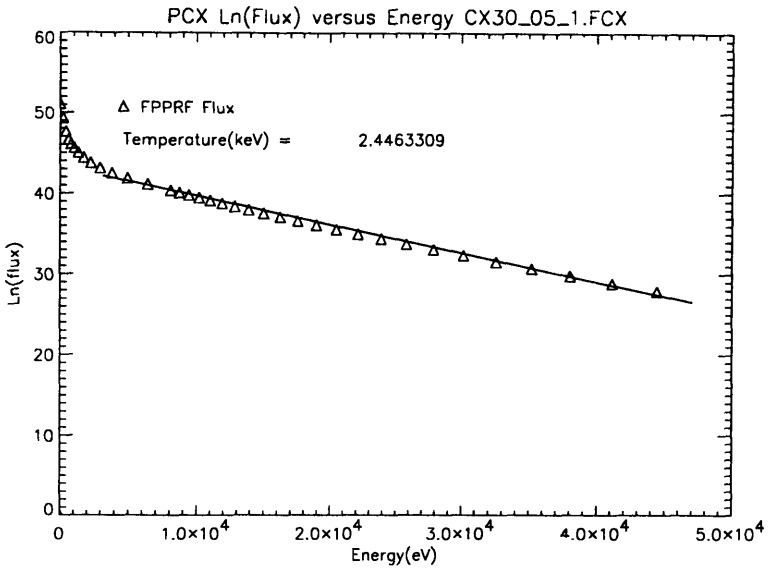

Figure 5-17: FPP Flux versus Energy with Fit

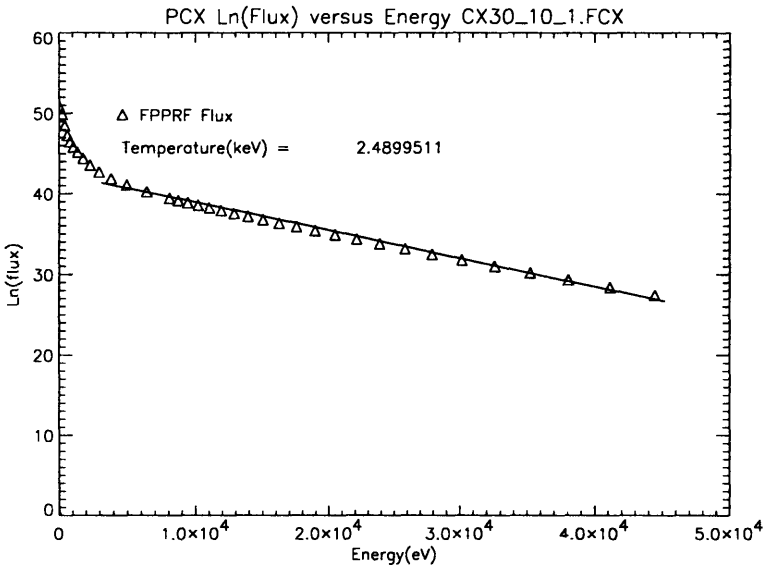

Figure 5-18: FPP Flux versus Energy with Fit

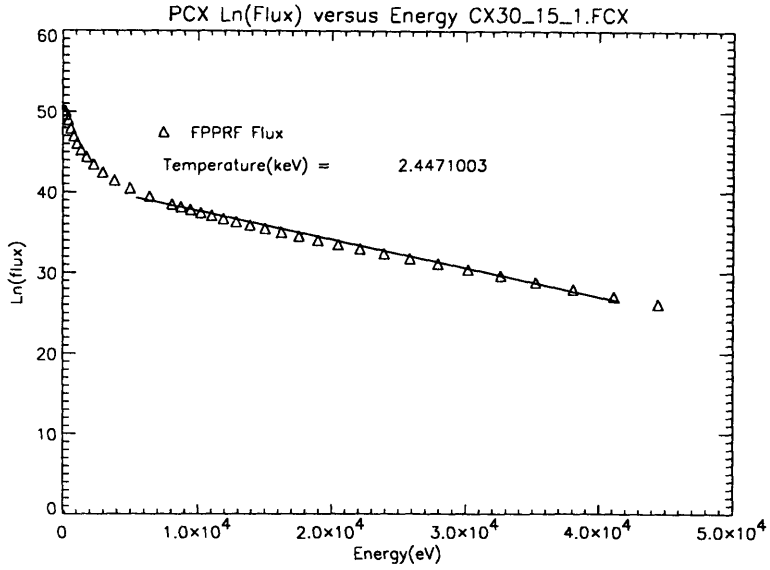

Figure 5-19: FPP Flux versus Energy with Fit

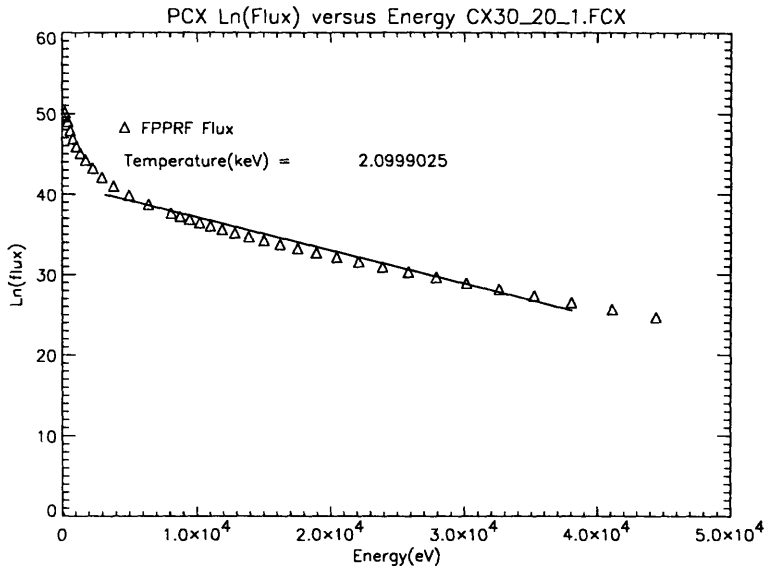

Figure 5-20: FPP Flux versus Energy with Fit

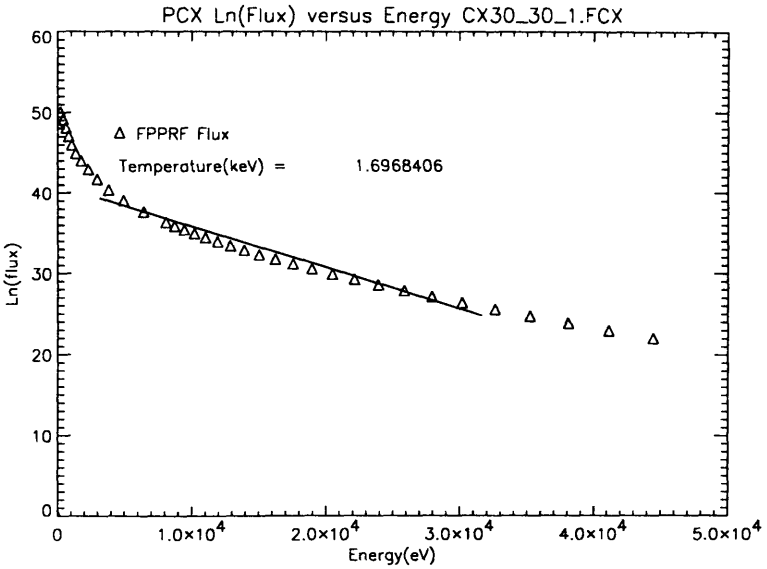

Figure 5-21: FPP Flux versus Energy with Fit

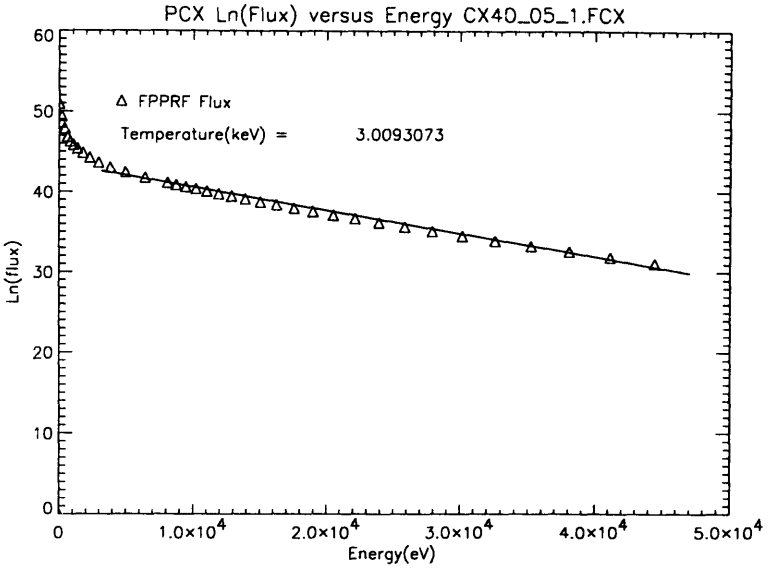

Figure 5-22: FPP Flux versus Energy with Fit

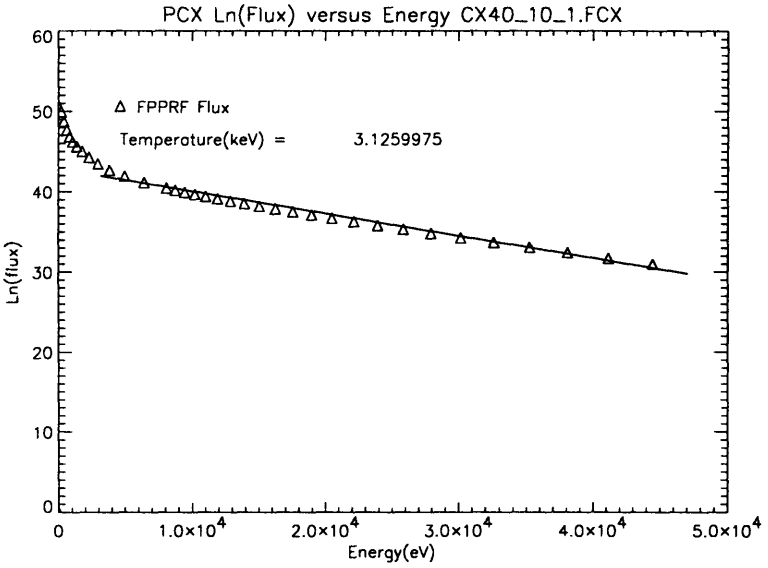

Figure 5-23: FPP Flux versus Energy with Fit

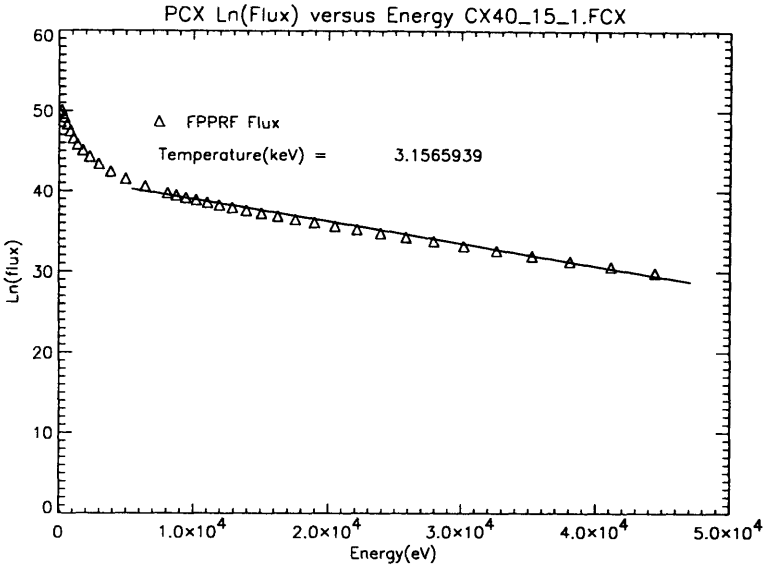

Figure 5-24: FPP Flux versus Energy with Fit

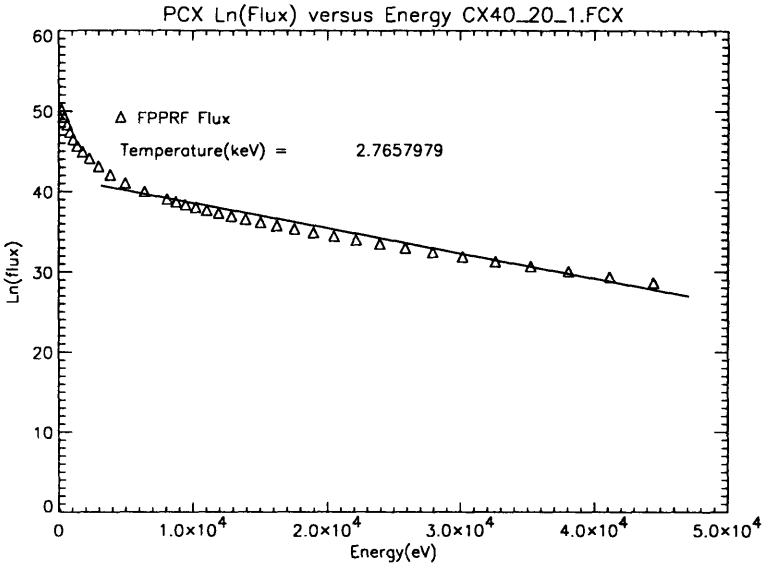

Figure 5-25: FPP Flux versus Energy with Fit

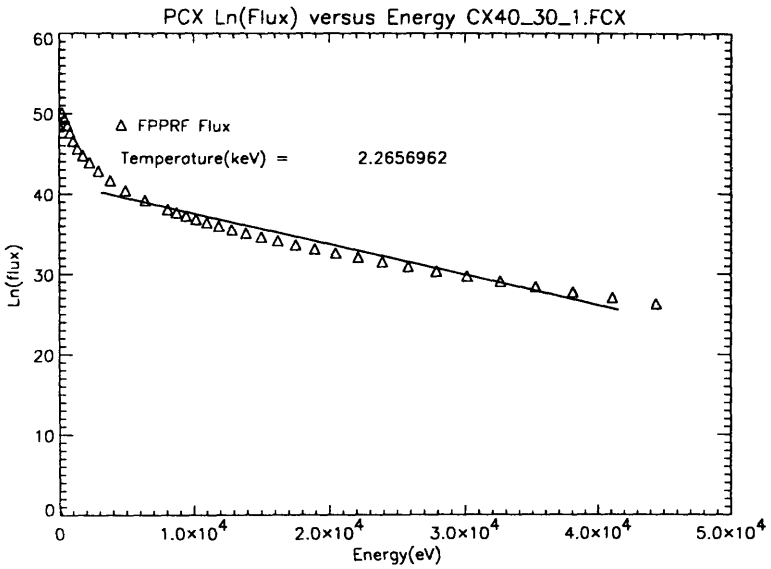

Figure 5-26: FPP Flux versus Energy with Fit

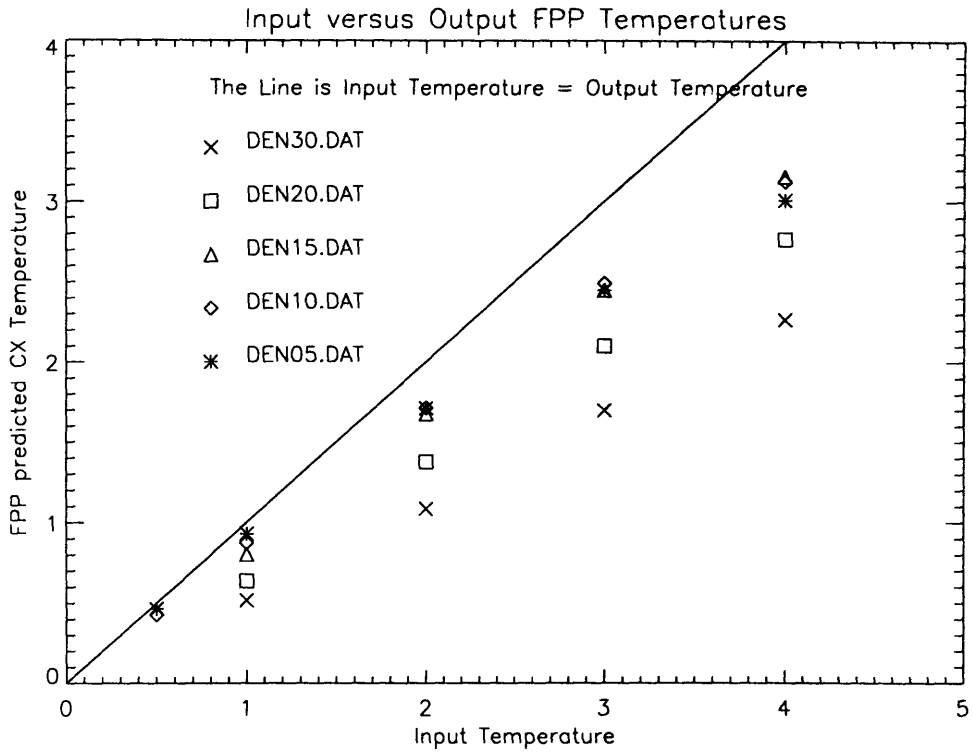

Figure 5-27: FPP Input versus Charge Exchange Measured Temperatures

Bibliography

[1] Ian Hutchinson, *The Physics and Engineering of Alcator C-MOD*, MIT PFC Report PFC/RR-88-11, Aug. 1988.

[2] Ian Hutchinson, Principals of Plasma Diagnostics, Cambridge University Press, 1987.

[3] S. L. Davis, D. Mueller, and C. J. Keane, *Mass Resolving Charge-Exchange System on the Poloidal Divertor Experiment*, Rev. Sci. Instrum. 54 (3), March 1983.

[4] M. R. C. McDowell and A. M. Ferendeci, Atomic and Molecular Processes in Controlled Thermonuclear Fusion, Plenum Press, 1980.

[5] R. L. Freeman and E. M. Jones, *Atomic Collision Processes in Plasma Physics Experiments*, CLM-R 137, 1974.

[6] J. H. Adlam and D. A. Aldcroft, *The Measurement of the Efficiency of a Helium Gas Cell for the conversion of a Beam of Energetic Hydrogen into a Proton Beam*, CLM-R 100, 1969.

[7] S. L. Davis, D. Mueller, and C. J. Keane, *The Mass Resolving Charge-Exchange System on PDX*, PPPL-1940, October 1982.

[8] A. L. Roquemore, G. Gammel, G. W. Hammet, R. Kaita, and S. S. Medley, *Application of an E||B Spectrometer to PLT Charge-Exchange Diagnostics*, Rev. Sci. Instrum. 56 (5), May 1985.

[9] Greg W. Hammet, *Fast Ion Studies of Ion Cyclotron Heating in the PLT Tokamak*, PhD Thesis, Princeton(1986).

[10] Joseph L. Wiza, *Microchannel Plate Detectors*, Nuclear Instruments and Methods 162, (1979) 587-601.